



# Parcel model for peak shapes in chromatography Numerical verification of the temporal distortion effect to peak asymmetry

Su-Cheng Pai\*

*Division of Marine Chemistry, Institute of Oceanography, National Taiwan University, P.O. Box 23-13, Taipei, Taiwan*

Received 5 November 2002; accepted 23 December 2002

## Abstract

The traditional plate concept has been reassessed and improved to a parcel matrix model, which can be used to imitate the chromatographic behavior of a hypothetical column on a computer worksheet. Under programmed conditions, various peak shapes (nearly Gaussian, and with prolonged or fronting tails) are generated. The peak tailing has been separated into two major fractions: spatial and temporal. The former fraction is caused by the retention nature of a column, whereas the latter is induced by the observer's relative position and the changing of the zone broadening rate. The temporal distortion effect can be identified qualitatively and quantitatively through a normalized peak-overlapping process. In general, a chromatographic peak may carry a prolonged (or normal type) tail under linear isotherms, while both prolonged and fronting tails will appear under non-linear conditions. The temporal distortion is proved to be significant, and may be regarded as the major cause of peak asymmetry in most cases. This is in contrast to the conclusions of many previous studies. The model is also eligible to simulate chromatographic peaks for various injection sizes.

© 2003 Elsevier Science B.V. All rights reserved.

**Keywords:** Parcel model; Peak shape; Temporal distortion effect; Peak tailing

## 1. Introduction

### 1.1. Peak shape problems

In analytical textbooks [1–3], the basic shape of a chromatographic peak is usually assumed to be “symmetrical” and can be approximated by a Gaussian equation. In practice, the peak shapes may not always be symmetrical. Skewed peaks do occur frequently in the laboratory, either with prolonged (normal type) or fronting (reverse type) tails.

Further discussion on the tailing phenomenon is diverse among different communities. Most routine analysts would regard the peak tailings as malfunctions or artifacts of the instrumentation, and ignore it because it does not affect the quantification. The plate numbers can still be estimated in an empirical way [4]. To simulate skewed peak shapes, several equations (e.g. the exponentially modified Gaussian, EMG) have been suggested [5–7]. The results have been claimed to be successful and useful in solving overlapped peaks on a chromatogram, regardless of the fact that small residuals between the modeled and experimental peaks are always present.

Theorists have shown much more interest in the

\*Tel.: +886-2-2362-7358; fax: +886-2-2363-2912.

E-mail address: [scpai@ccms.ntu.edu.tw](mailto:scpai@ccms.ntu.edu.tw) (S.-C. Pai).

modeling of peak tails. Although some potential sources that can cause peak deformation have been identified [8,9], explanations are somewhat vague and difficult to understand. Peak asymmetry problems, especially peak fronting, remain puzzling.

It is deemed that something in the existing theories might have been misinterpreted or overlooked. The most possible suspect would be the “temporal distortion effect” [10]. If this effect has been proved to exist in a flow injection system, it must also occur in chromatography.

### 1.2. The fractions of tailing

A peak tail can comprise two major fractions: spatial and temporal. In the past, the spatial fraction was considered exclusively responsible for the tailing. The focus has been on the uneven packing of resin in a column, shapes of detector, tube wall friction effects, etc. The temporal fraction, on the contrary, has seldom been mentioned or discussed in the literature.

The temporal contribution to the peak tailing may be described by a concept of relativity [10]: when a shape-changing subject (symmetrical or not symmetrical) passes through a single fixed position detector, the observer will receive a distorted pattern from the real image of that subject at a specific time. For column-type chromatography, the detector is usually located at the outlet of the column, which records signals when the sample zone passes through. If the zone broadening rate ( $d\sigma/dt$ ) in the column is large, the resultant chromatographic peak will be distorted regardless of whether or not the mass pattern is symmetrical. On the recorder, the temporal fraction of a tail is spatially *false*.

### 1.3. False tailing in diffusion models

It is not difficult to find evidence of the false tailing fraction in previous diffusion models. In those models, the formation of a peak in a chromatographic column is considered as the “broadening” of the sample zone (in terms of peak width  $W$  or standard deviation  $\sigma$ ) by a number of mechanisms [1,2]. Mathematically it can be expressed as:

$$\sigma_L^2 = \sigma_{\text{initial}}^2 + \sigma_{\text{diffusion}}^2 + \sigma_{\text{retention}}^2 + \dots \quad (1)$$

where  $\sigma_L$  is the standard deviation of a sample zone on the longitudinal coordinate ( $L$  axis), resulting from the accumulation of the initial zone width, the effect of mass diffusion, the effect of retention by the stationary phase, and other physical effects such as non-equal path, extra-column, etc. By combining all mechanisms as a whole, the distribution can be approximated as a peak function by taking the solution of Fick's law ( $\partial C/\partial t = D \partial^2 C/\partial L^2 - u_x \partial C/\partial L$ , where  $D$  is the empirical diffusion coefficient of the system,  $u_x$  the migration speed of an analyte  $X$ ) to generate a Gaussian-type distribution curve or the concentration profile,  $C(L)$ , on the  $L$  coordinate [11]:

$$C(L) = \frac{C_o W_o}{\sqrt{2\pi} \sigma_L} e^{-(L-u_x t)^2/2\sigma_L^2} \quad (2)$$

where  $C_o$  and  $W_o$  are the initial concentration and zone width of the injected sample;  $t$  the time duration, and  $\sigma_L = \sqrt{2Dt}$ . The curve plotted for Eq. (2) at a selected time is a Gaussian peak, which is usually named the mass distribution pattern.

If this pattern is to be observed by a detector, the coordinate should be transferred to a time scale, i.e. plotted for  $C(t)$  instead of  $C(L)$ . By treating  $L$  as a constant and time a variable, the curve plotted for  $C(t)$  would turn from “symmetrical” to “not symmetrical” [12,13]. A tail is generated, not in the space domain, but in a time domain. It should be named the temporal tailing.

In practice, it is still difficult to distinguish the two tailing fractions just from the peak appearance. Although most analysts would prefer to solve the peak asymmetry problems directly from the diffusion equations, it should be noted that the coefficient  $D$  in Eq. (2) comprises both diffusion and retention terms. The diffusion effect is unlikely to cause a peak to be asymmetrical. On the contrary, it diminishes rather than generates the asymmetry of a peak. Therefore the diffusion approach sometimes might cause the problem to be more ambiguous. In this respect, the original plate concept [14,15], which focuses “only” on the retention effect, is more straightforward and practical.

### 1.4. False tailing in plate models

Several practical plate models have been sug-

gested previously, including the dynamic plate model by Glueckauf [16] and the statistic plate model suggested by Fritz and Scott [17]. In those models, the mass distribution patterns and the chromatographic peaks (or the exit time curve), are all not symmetrical at initial stages or when the plate number is small. However, those authors did not pay too much attention to the peak asymmetry problem. Their conclusions are made on the symmetrical side: the peak shape will soon turn to a Gaussian curve when the plate number increases; the tailing will be insignificant and not important at large plate numbers.

Since the temporal distortion fraction has never been separated and discussed individually, the author believes that it could be the key to the deciphering of the peak asymmetry puzzle. It is very possible that all types of peak tailings (prolonged or fronting) have already been endorsed in the plate concept, but have yet to be interpreted appropriately. A detailed reassessment on those plate models is deemed necessary.

### 1.5. Focus of this study

The targets of the present study are to improve the plate model so that spatial and temporal tailing fractions can be verified separately, and to exemplify possible situations that may cause prolonged and fronting peaks. In combination it is expected to provide analysts with a practical tool for simulating, predicting and solving chromatographic peaks before and after commencing an experiment. The skills of using a computer worksheet as suggested by de Levie [18,19] were generally adopted, but expanded to include various isotherms. A “parcel” concept has been proposed, which enables the contribution of the temporal distortion effect to be more clearly displayed.

## 2. Theoretical

### 2.1. Equilibrium in a plate

In plate theory [14], a “plate” is a unit section or layer of a narrow column. For partition chromatography the equilibrium within a plate should obey the

following isotherm (at a constant temperature):  $K = C_s/C_m$ , where  $K$  is the distribution constant,  $C_s$  and  $C_m$  are the concentrations of a substance in the stationary and mobile phases, respectively. The equilibrium can also be described in a mass unit if taking the volume factor to be constant:

$$k' = m_s/m_m \quad (3)$$

where  $k'$  is the mass partition ratio between the two phases, which is frequently termed the capacity ratio of a substance in a column.

Since the complete partition equilibrium can “never” be achieved, an apparent or dynamic partition ratio  $k''$  is introduced:

$$k'' = d_u k' \quad (4)$$

where  $d_u$  is the degree of completeness of the equilibrium (ranges 0–1) at a given flow speed  $u$ . It may be described as an exponential function of the equilibrium time ( $t_{eq}$ ) in a plate, which is a reciprocal function of the flow speed  $u$ . When the effluent flows very slowly,  $d_u$  approaches 1 and  $k'' \approx k'$ ; whereas when the flow is at a fast speed, both  $d_u$  and  $k''$  can be very small.

At constant flow speed,  $k''$  can be influenced by temperature and the composition of the mobile effluent. In many applications these conditions are programmed to change in order to obtain optimal separations (e.g. the elevation of temperature for GC and the changing of effluent composition for HPLC). Under these non-linear conditions, the partition ratio  $k''$  becomes a variable with time and should be denoted as  $k''(t)$ .

### 2.2. The parcel concept

To advance the plate equilibrium continuously along a column, Glueckauf [16] added a “time” label to each plate to show its location along the time coordinate. To further expand the usage of this concept, the “time-labeled plate” has been regarded as a “parcel” in this paper.

A parcel is defined as a unit section of a column at a particular moment. Allowing the column length  $L$  to be separated into many small sections,  $L = n\Delta L$ , and the time duration  $t$  to be divided into many small time steps,  $t = \tau\Delta t$ , each parcel is denoted as  $P(n,\tau)$  with a section number  $n$  and a time step number  $\tau$ .

The  $n \times \tau$  parcel matrix imitates the entire column operation over the time duration, and a parcel is the minimal fraction unit of this matrix.

The mean flow velocity ( $u$ ) of the mobile effluent is defined to be  $u = L/t = n\Delta L/\tau\Delta t$ , or  $u = n/\tau \times \Delta L/\Delta t$ . Since the calculation is made “section-by-section” and “step-by-step”, and  $n$  and  $\tau$  are all integers, a dimensionless flow velocity  $v$  is defined to be 1 for the discrete calculation on the parcel matrix.

### 2.3. Mass flux balance in a parcel

The complete mass balance for a given parcel  $P(n, \tau)$  can be expressed in terms of mass fluxes ( $F_i$ , the mass changes per time step, see Fig. 1):

$$\begin{aligned} F_{\text{incoming}} &= F_1 + F_2 + F_3 + F_4 = F_{\text{output}} \\ &= F_5 + F_6 + F_7 + F_8 \end{aligned} \quad (5)$$

The total incoming flux for  $P(n, \tau)$  includes:  $F_1$ , the stationary mass transported from  $P(n, \tau - 1)$ ;  $F_2$ , the mobile mass transported from  $P(n - 1, \tau - 1)$ ; and  $F_3$  and  $F_4$ , the mass diffused from  $P(n - 1, \tau - 1)$  and  $P(n + 1, \tau - 1)$ . The magnitude of the diffusion flux

is decided by a diffusion coefficient  $D$  and the gradients between parcel pairs, e.g.  $P(n - 1, \tau - 1)/P(n, \tau - 1)$  and  $P(n, \tau - 1)/P(n + 1, \tau - 1)$ .

The total mass within a parcel  $P(n, \tau)$  is marked as  $m_{t(n, \tau)}$ , and it can be split into the stationary and mobile phases, i.e.  $m_{s(n, \tau)}$  and  $m_{m(n, \tau)}$ , respectively, according to the dynamic equilibrium at a given time step:

$$k''(\tau) = \frac{m_{s(n, \tau)}}{m_{m(n, \tau)}} \quad (6)$$

The total incoming mass is re-distributed into the two phases:

$$m_{s(n, \tau)} = m_{t(n, \tau)} \times k''(\tau) / [k''(\tau) + 1] \quad (7)$$

$$m_{m(n, \tau)} = m_{t(n, \tau)} / [k''(\tau) + 1] \quad (8)$$

After the equilibrium, the mass fluxes that leave the parcel  $P(n, \tau)$  are:  $F_5$ , the stationary fraction mass transported to  $P(n, \tau + 1)$ ;  $F_6$ , part of the mobile fraction mass transported to  $P(n + 1, \tau + 1)$ ; and  $F_7$  and  $F_8$ , part of the mobile-phase mass diffused to  $P(n + 1, \tau + 1)$  and  $P(n - 1, \tau + 1)$ , respectively.

### 2.4. Simplified parcel matrix

The reproduction of a single parcel to an  $n \times \tau$  matrix gives a cross-linked structure, which indicates all possible mass transportation routes in the column operation. However, the calculation can be quite complex if the diffusion fluxes are included. As mentioned in Section 1.3, the addition of the diffusion terms does not really help an analyst to answer: “why is the peak shape not symmetrical?”. For these reasons, the parcel matrix is simplified by deleting all diffusion fluxes and leaving only the transportation routes for the stationary and mobile phases (Fig. 2). However, it is still possible to add the diffusion effect later as a modification, after the basic peak shape has been generated (please note that a diffusion modification will make the peak slightly wider, but will not affect the trend of the skewness).

Thus, the simplified mass balance for a parcel  $P(n, \tau)$  becomes:

$$m_{s(n, \tau-1)} + m_{m(n-1, \tau-1)} = m_{s(n, \tau)} + m_{m(n, \tau)} \quad (9)$$

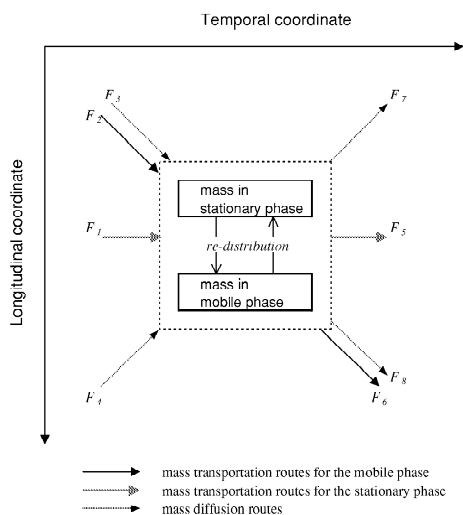


Fig. 1. Mass flux balance of a single parcel on the longitudinal–temporal dimensions. The total incoming mass received from the left parcels ( $F_{\text{incoming}} = F_1 + F_2 + F_3 + F_4$ ) is re-distributed into stationary and mobile phases, and they are delivered out to the parcels on the right ( $F_{\text{output}} = F_5 + F_6 + F_7 + F_8$ ); where  $F_{\text{incoming}} = F_{\text{output}}$ .

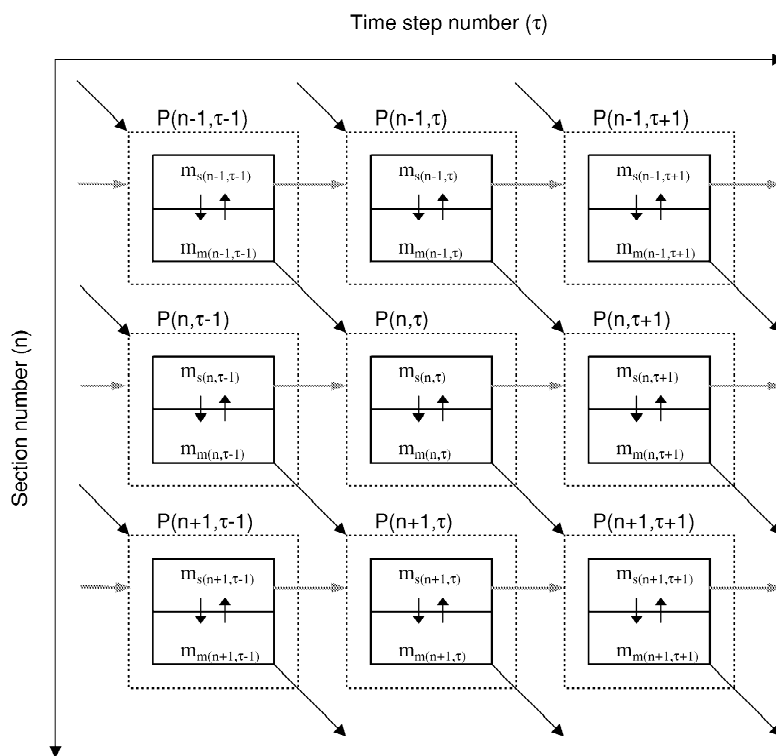


Fig. 2. A simplified longitudinal–temporal parcel matrix formed by cross-linking the transportation routes for the stationary and mobile phases and deleting (for clearance) the possible mass diffusion routes.

Accordingly, a “unit” parcel contains just two calculation terms:

$$m_{s(n, \tau)} = [m_{s(n, \tau-1)} + m_{m(n-1, \tau-1)}]k''(\tau) / [k''(\tau) + 1] \quad (10)$$

$$m_{m(n, \tau)} = [m_{s(n, \tau-1)} + m_{m(n-1, \tau-1)}] / [k''(\tau) + 1] \quad (11)$$

The same conditions apply to all parcels on the matrix. The directions of the calculation (delivery of values) are horizontally for the stationary phase and diagonally for the mobile phase.

### 2.5. Parcel matrix on worksheet

The parcel matrix can be displayed on a computer worksheet, e.g. Microsoft Excel. The recursion treatment is quite similar to that suggested by de Levie [18]. Each parcel occupies two worksheet cells, the

upper one for  $m_{s(n, \tau)}$  and the lower for  $m_{m(n, \tau)}$ . The unit parcel is copied both longitudinally (vertically down) and temporally (horizontally right) to give an  $n \times \tau$  matrix (see Fig. 3 for a  $6 \times 6$  example).

Two additional parcel sets are also created. The parcel set from  $P(1,0)$  to  $P(n,0)$  imitates the initial state of the virtual column; and the other from  $P(0,0)$  to  $P(0,n)$  is reserved for the hypothetical injector.

### 2.6. Injection size

The size of the injector on the matrix is usually unique, but can be optional and adjustable. For a single impulse injection, the injector occupies only one parcel at  $P(0,0)$ . To double the sample size, it occupies two parcels from  $P(0,0)$  to  $P(0,1)$ . For frontal analysis or pre-concentration simulations in which the sample is loaded continuously, the injector can be further expanded to the right end of the matrix.

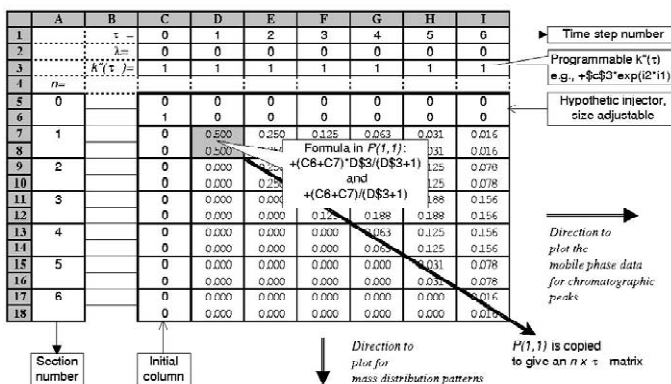


Fig. 3. Setting up of an  $n \times \tau$  parcel matrix on the Microsoft Excel worksheet by copying the recursion equations within a unit parcel (e.g. in  $P(1,1)$ ) along both coordinates. Each parcel occupies two worksheet cells (the upper for the stationary phase and the lower for the mobile phase). The hypothetical injector occupies a row of parcels from  $P(0,0)$  to  $P(0,\tau)$  depending on the sample size. If a single impulse is needed then a mass value is filled into the mobile phase cell of  $P(0,0)$ . The redistribution equilibrium is governed by  $k''(\tau)$ , which is variable with time step and can be programmed (in the 3rd row cells) to be consistent, stage-wise or continuous decreasing.

2.7. Programmable  $k''(\tau)$

The  $k''(\tau)$  value can be programmed, as either consistent, stage-wise decreasing or continuous decreasing. For linear isotherms, the  $k''(\tau)$  values for all time steps are the same (filled all cells with the same value). For stage-wise changing, different values can be filled for several time step periods, e.g.  $k''(\tau) = k''_1$  from  $\tau_0$  to  $\tau_1$ ,  $k''(\tau) = k''_2$  from  $\tau_1$  to  $\tau_2, \dots$  etc. In many circumstances the changing of isotherm can be made continuously, either in a “direct” or “exponential” relationship to the time step. For this, one may choose either of the following equations and fill into the corresponding cells on the worksheet:

$$k''(\tau) = k''_0(1 - \lambda\tau) \quad 0 \leq \lambda\tau \leq 1 \tag{12}$$

or,

$$k''(\tau) = k''_0 e^{-\lambda\tau} \tag{13}$$

where  $\lambda$  is the decay constant. To simulate GC operation the latter equation is much more preferable, as the dropping of  $k''(\tau)$  is in a reciprocal relationship to the temperature elevation rate ( $dT/d\tau$ ). On the matrix, Eqs. (12) and (13) can also be written in recursion forms as:  $k''(\tau) = k''(\tau - 1) - \lambda$  and  $k''(\tau) = k''(\tau - 1)(1 - \lambda)$ , respectively.

2.8. Operating the parcel matrix

The procedures of operating the parcel matrix are as follows.

1. Define the status of the isotherm by inputting a value for the decay constant ( $\lambda$ ). In linear cases,  $\lambda = 0$ .
2. Input an initial  $k''_0$  value at  $\tau=0$ ; then fill other  $k''(\tau)$  cells with desired values or copy an equation to the entire time step duration. In linear cases,  $k''(\tau) = k''_0$ .
3. For a single impulse, fill a mass value for  $m_{m(0,0)}$  in  $P(0,0)$ . If the injector occupies more than one parcel, fill all other parcels with the same values. Once the injection has been done, the worksheet generates immediately two data ( $m_s$  and  $m_m$ ) for each parcel and fills automatically the whole  $n \times \tau$  parcel matrix.
4. Select a time  $\tau$  to view the mass distributions: the data sets in the vertical parcel column  $P(n,\tau)$  are used for plotting three “mass distribution profiles” along the  $n$  coordinate, namely, the mass in the stationary phase, mobile phase, and total (sum of both).
5. Select a longitudinal position to view the “elution profile” or “chromatogram”. The chromatographic peak, if observed by a hypothetical detector located at a position  $n = N$ , refers to the

$m_{m(N, \tau)}$  data (mobile phase only) in the horizontal parcel set  $P(N, \tau)$ . The diagram is plotted along the  $\tau$  coordinate.

6. If  $\Delta L$  and  $\Delta t$  have been defined (e.g.  $\Delta L = 1$  cm;  $\Delta t = 1$  s, or else), then the above dimensionless plots can be transformed to  $L$  or  $t$  coordinates.

### 2.9. Peak parameters on matrix

Following the above procedures, two types of diagrams (spatial and temporal) can be generated. The definitions of the peak parameters are described separately as follows.

1. Along the  $n$  coordinate, at a selected  $\tau$ .

- Mass peak heights ( $h_t, h_s, h_m$ ): the maximum mass values (refer to total, stationary and mobile phases, respectively) that appear in a vertical parcel set at a selected time step.
- Mass peak position ( $n_p$ ): the section number that contains the maximum mass values (mass maxima for the stationary and mobile phases are synchronized).
- Arrival time of the mass peak ( $\tau_{rm}$ ): for a fixed column length, the total time step required for the mass peak to arrive at the detector.
- Band broadening rate: mathematically defined following the suggestion by Fritz and Scott [17]:

$$\frac{\Delta\sigma_n(\tau)}{\Delta\tau} = \frac{\sqrt{k''(\tau)}}{k''(\tau) + 1} \quad (14)$$

- Standard deviation of the sample zone ( $\sigma_n(\tau)$ ): on the worksheet, the recursion calculation formula can be written as:

$$\sigma_n(\tau) = \sqrt{\sigma_n(\tau - 1)^2 + \Delta\sigma_n^2} \quad (15)$$

- Peak width on  $n$  coordinate ( $W_n(\tau)$ ): it is defined as  $W_n(\tau) = 4\sigma_n(\tau)$ .

2. Along the  $\tau$  coordinate, at a selected  $n$ .

- Chromatographic peak height ( $h_r$ ): the maximum value found in the “mobile phase cells” of the horizontal parcel set.
- Chromatographic peak position ( $\tau_r$ ): the equivalent to the traditional “retention time” of a peak that appears on the recorder chart. It does not equal  $\tau_{rm}$  by definition.
- Appeared peak standard deviation ( $\sigma_r(\tau_{rm})$ ):

although the peak appears at  $\tau_r$ , its theoretical standard deviation should still refer to the mass position at  $\tau_{rm}$ , and is estimated by:

$$\sigma_r(\tau_{rm}) \approx \sigma_n(\tau_{rm})(k''(\tau_{rm}) + 1) \quad (16)$$

3. On the matrix.

- The migration speed ( $v_m(\tau)$ ): the rate of longitudinal movement of the mass center per time step, defined as:

$$v_m(\tau) = \frac{\Delta n_p(\tau)}{\Delta\tau} = \frac{1}{k''(\tau) + 1} \quad (17)$$

The highest migration speed is 1 when  $k''(\tau) = 0$ , and becomes near zero when  $k''(\tau)$  is very large.

- The migration route of the mass center ( $n_p(\tau)$ ): it is obtained by a recursion calculation on the parcel matrix:

$$n_p(\tau) = n_p(\tau - 1) + \Delta n_p \quad (18)$$

- The migration slope (or  $\tau/n$  ratio): a reciprocal function of migration speed  $v_m(\tau)$ , or  $\tau/n(\tau) = k''(\tau) + 1$ .
- Peak locations: for a given column length  $N$ , the migration route curve crosses the horizontal  $n = N$  line at the parcel address  $P(N, \tau_{rm})$ ; whereas the chromatographic peak is seen at the address  $P(N, \tau_r)$ . The two addresses coincide only when  $k''(\tau)$  is zero or very small.

### 2.10. Overlapping the spatial and temporal peaks

Although the mass pattern should never be observed by a single detector, it can be displayed hypothetically by the matrix. It would be interesting to find out how will this pattern be twisted if it were seen by a detector. This offers a quantitative measure of the temporal distortion effect.

However, the spatial and temporal peaks cannot be plotted directly on the same coordinate, and a normalization process must be taken. The major concerns are the mirror image effect due to the observing position, and the expanding effect due to the migration speed. To compensate for these effects, the  $n$  coordinate should be firstly converted to  $2N - n$  coordinate, and then multiplied by a factor  $k''(\tau_{rm}) + 1$ .

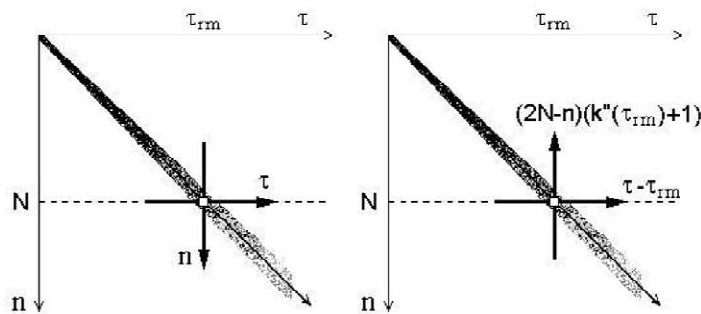


Fig. 4. Axial transformations for the overlapping of the spatial profile and temporal peak at the mapping center  $P(N, \tau_{rm})$ . Left, collect mobile-phase mass data along  $n$  and  $\tau$  coordinates. Right, re-plot data on the normalized  $(2N-n)(k''(\tau_{rm})+1)$  and  $\tau - \tau_{rm}$  coordinates, and then overlap the two diagrams.

The mapping procedures are suggested below (also see Fig. 4).

- Step 1 For a given column length  $N$ , locate the address  $P(N, \tau_{rm})$  as the mapping center for both peaks.
- Step 2 Obtain “only” the mobile-phase mass values (together with their corresponding  $n$  or  $\tau$  scaling values) along the vertical column and horizontal row.
- Step 3 Re-plot the vertical mass values on the  $(2N-n)(k''(\tau_{rm})+1)$  coordinate.
- Step 4 Re-plot the horizontal mass values on the  $t - t_{rm}$  coordinate.
- Step 5 Overlap the two re-plotted peaks on one diagram.

The difference (or the residual curve) between the normalized spatial and temporal curves gives the “net” temporal distortion effect.

### 3. Numerical demonstration under linear isotherms

#### 3.1. Demonstration of a single impulse injection

A  $30 \times 50$  parcel matrix was found to be convenient to illustrate the shape of a single peak under linear isotherms, i.e.  $\lambda=0$  and  $k''(\tau) = k''$ . In this section six  $k''$  values (i.e.  $k'' = 0.1, 0.2, 0.5, 1, 2$  and  $5$ ) were used. The injector occupied one parcel, and the injected mass number ( $m_o$ ) was 1. Mass distributions were examined at  $\tau=10, 20$  and  $30$ , respectively (Fig. 5); whereas chromatographic

peaks were plotted for detectors at  $n=5, 10$ , and  $15$ , respectively (Fig. 6).

#### 3.2. General aspects of the linear parcel model

Under linear isotherms, and if the sample size injected is limited to a “single impulse”, the present parcel matrix model is no different from that suggested by de Levie [18,19]. It is also equivalent to the binominal equations that derived from a statistical discrete plate model by Fritz and Scott [17]. Thus, the masses contained within a parcel at any given address  $P(n, \tau)$  can also be expressed as:

1. in stationary phase:

$$m_{s(n, \tau)} = m_o \frac{(\tau-1)!}{(\tau-n)!(n-1)!} \left( \frac{k''}{k''+1} \right)^{\tau-n+1} \left( \frac{1}{k''+1} \right)^{n-1} \quad (19)$$

2. in mobile phase:

$$m_{m(n, \tau)} = m_o \frac{(\tau-1)!}{(\tau-n)!(n-1)!} \left( \frac{k''}{k''+1} \right)^{\tau-n} \left( \frac{1}{k''+1} \right)^n \quad (20)$$

3. the total (sum of both phases):

$$m_{t(n, \tau)} = m_o \frac{(\tau-1)!}{(\tau-n)!(n-1)!} \left( \frac{k''}{k''+1} \right)^{\tau-n} \left( \frac{1}{k''+1} \right)^{n-1} \quad (21)$$

where  $n, \tau, \tau - n > 0$ . Plotting of these equations,

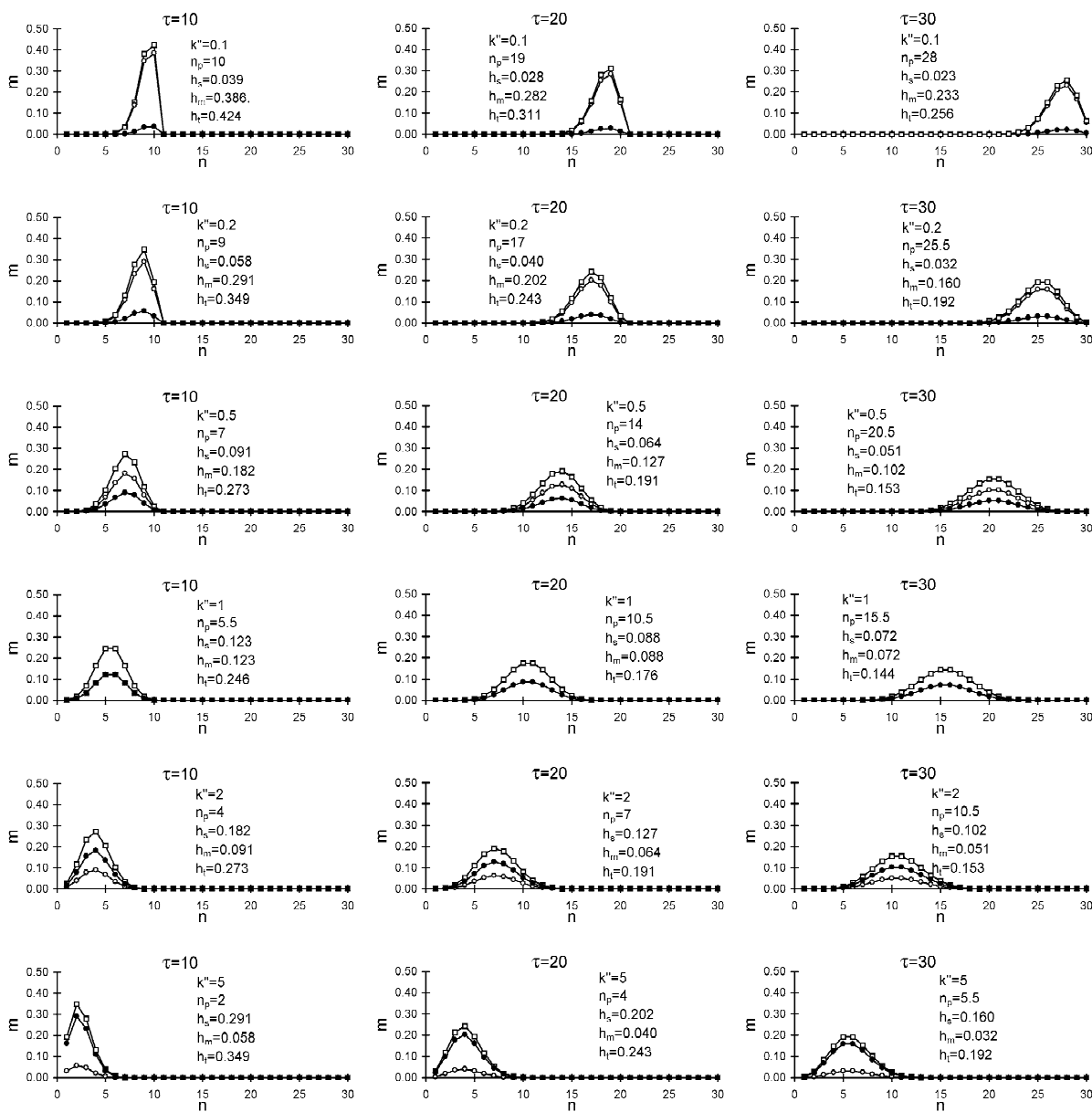


Fig. 5. Mass distribution patterns for the stationary phase ( $m_s$ , solid circle), mobile phase ( $m_m$ , open circle) and total ( $m_t = m_s + m_m$ , open cube) along the  $n$  coordinate under linear isotherms. Data are calculated at  $\tau = 10, 20$  and  $30$ , respectively, with various  $k'$  values. The position of the mass center  $n_p$  as well as the corresponding heights for  $h_s, h_m$  and  $h_t$  are also given to each mass peak.

e.g.  $m_t(n)$  or  $m_m(n)$ , along the  $n$  coordinate at a given  $\tau$  gives the mass distribution patterns. Plotting of Eq. (20) in the form  $m_m(\tau)$  along the  $\tau$  coordinate for a column length  $n = N$  gives the chromatographic peak.

Even though those authors have discussed the general features of the chromatographic peak shapes previously, it is still worthwhile to re-examine the peak parameters in both spatial and temporal coordinates, and to find the differences between the two.

### 3.3. Mass profiles

The mass profiles shown in Fig. 5 clearly indicate that they are influenced by both the  $k''$  value and observation time in terms of shape, position, as well as the peak height. For the single impulse injection, the “ $k'' = 0$ ” and “ $k'' = 1$ ” are decisive boundaries controlling the skewness of a mass peak:

1. when  $k'' = 0$ , the mass will not enter the stationary phase at any time, and will appear at the void position without shape-changing;
2. when  $0 < k'' < 1$  the mass distributes more in the mobile phase, and the migration speed is relatively fast. The patterns for the mobile phase, stationary phase, as well as the sum of both, all look non-symmetrical. The skewness is more obvious when  $k''$  is very small or near zero, the peaks lean slightly toward the right on the chart (a mirror image of a normal-type tailing), and the peak positions are close to the void position;
3. when  $k'' = 1$  the mass distributes evenly between the stationary and mobile phases and the patterns are completely symmetric over the entire time duration;
4. when  $k'' > 1$ , the situations invert to  $k'' < 1$ . More mass fraction tends to stay in the stationary phase. The peaks lean toward the left (a mirror image of a fronting-type tailing) and the migration along the column is relatively slow.

It is also found that the total mass curves for  $k'' = 0.2$  and 5 are mirror images of each other, so as for  $k'' = 0.5$  and 2, and every  $k''$  and  $1/k''$  pairs. The difference would be that the proportions of the mass in the stationary and mobile phases are reversed.

If the injector size were larger than one parcel, the general trends as stated above are still applicable; only the patterns for  $k'' = 1$  are no longer completely symmetrical in the starting stage.

### 3.4. Position of mass peaks on the matrix

The location of the maximum mass values in the vertical parcel set is the position of the mass peak. It may not necessarily be found in a single parcel because sometimes the values for two adjacent parcels are identical. In this case a 0.5 unit is employed to address the peak position.

If  $k''$  is constant, the maximum mass value ex-

pands like a ridge on the matrix. The migration speed is  $v_m = 1/(k'' + 1)$ , and the  $\tau/n$  slope is  $k'' + 1$ . Ideally, for the single impulse injection, the migration route should be described by  $n_p = v_m \tau$ . However, this is obeyed only when  $k'' = 0$ ; a consistent shift is found for those  $k'' > 0$ . For example, when  $k'' = 1$ , the mass maxima are found in the parcels of  $P(1,1)$ ,  $P(1.5,2)$ ,  $P(2,3)$ ,  $P(4,7)$ ,  $P(6,11)$ ,  $P(10,19)$ , ... etc., and the migration route becomes:

$$n_p(\tau) = \tau/(k'' + 1) + 0.5 \quad (22)$$

The 0.5 is named the “longitudinal shift”, a practical term for the parcel matrix. The shift is because the injected size is not zero but  $1\Delta L$ , therefore the initial mass center is at the +0.5 position on the  $n$  coordinate. To show the peak position on a matrix, the  $n_p$  value of Eq. (22) should be rounded off to the nearest integer unless with a decimal value of exactly 0.5 (at which the mass center lies exactly between two parcels). For example, if  $\tau = 20$  and  $k'' = 0.1$ ; the value for  $n_p(20)$  is 18.68 and the mass center will appear in parcel  $P(19,20)$ ; when  $k'' = 0.2$ ,  $n_p(20) = 17.17$ , the mass center will be in parcel  $P(17,20)$ ; when  $k'' = 1$ ,  $n_p(20) = 10.5$ , the mass center lies between  $P(10,20)$  and  $P(11,20)$ .

The time required for a mass center reaching the end of a column (length  $N$ ) is marked as  $\tau_{rm}$ :

$$\tau_{rm} = (N - 0.5)(k'' + 1) \quad (23)$$

When the column is long, the 0.5 shift may no longer be important and the equation will appear similar to that found in textbooks. However, it should be emphasized that  $\tau_{rm}$  should not be treated as the conventional retention time  $\tau_r$  for a chromatographic peak.

Again, Eqs. (22) and (23) are valid for the single impulse injection only. The increase of sample size will cause an extra delay for both  $n_p$  and  $\tau_{rm}$ .

### 3.5. Zone broadening on the $n$ coordinate

In principle, the broadening of a sample zone is a function of the square root of time step number  $\tau$ , as stated in Eq. (15). However, since the initial sample zone on the matrix is not zero, an initial  $\sigma_n(0)$  value of 0.34 should be included:

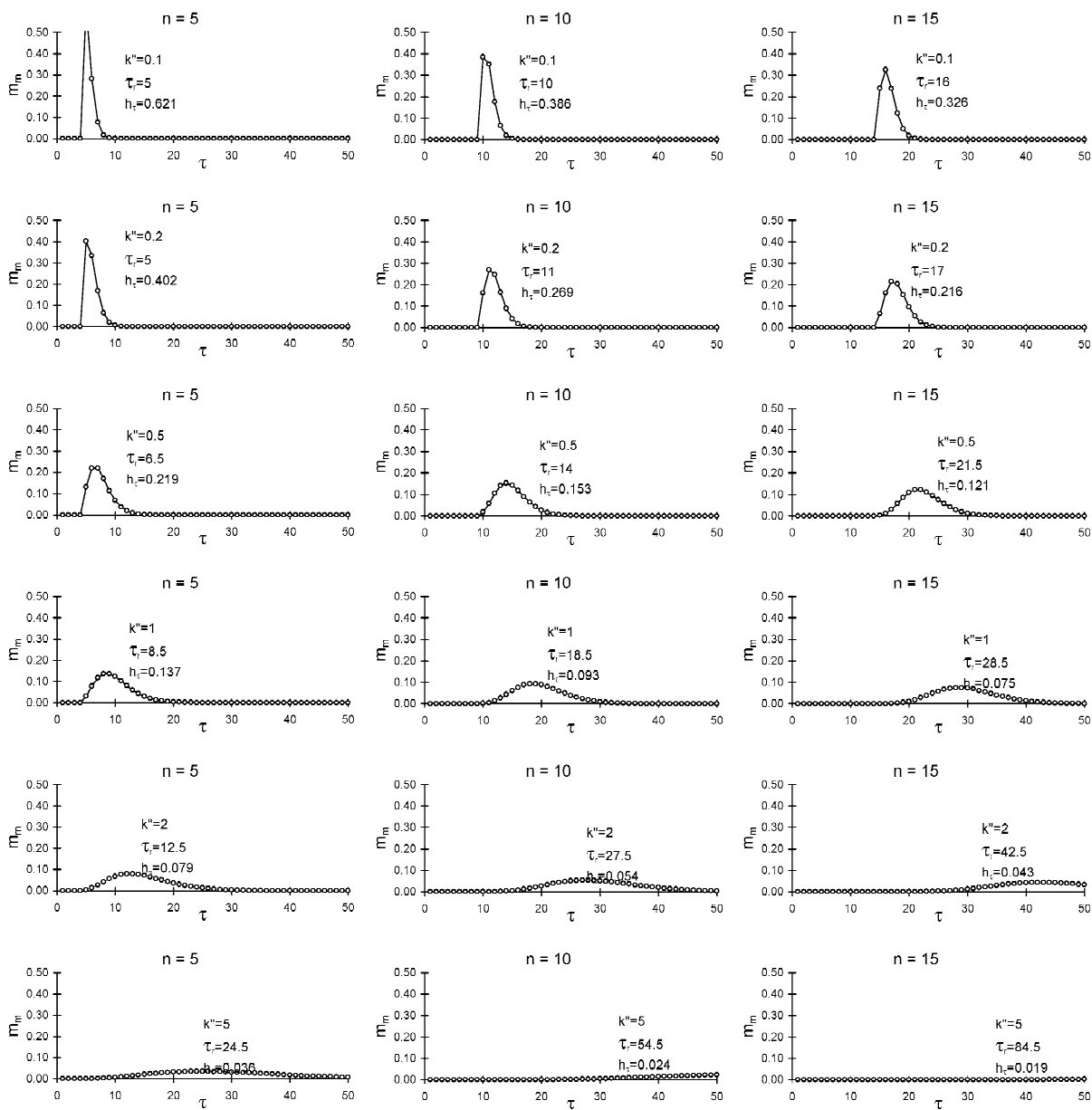


Fig. 6. Chromatographic peaks (with various  $k''$ ) observed at positions  $n=5, 10$  and  $15$ , respectively, under linear isotherms. The retention time ( $\tau_r$ ) and peak height ( $h_r$ ) are labeled on each diagram. The peak tailing is induced by a combined effect of the asymmetry of the mass distribution and the non-simultaneous detection. At  $k'' = 1$  the asymmetrical tailing should attribute exclusively to the latter.

$$\sigma_n(\tau) = \sqrt{0.34^2 + \left(\frac{\sqrt{k''}\tau}{k'' + 1}\right)^2} \quad (24)$$

The standard deviations for the total, stationary,

and mobile phase peaks are identical. The widest zone width in a column occurs when  $k'' = 1$ . For example, at  $\tau=20$ ,  $k'' = 0.1, 0.2, 0.5, 1, 2$  and  $5$ , the standard deviations  $\sigma_n(20)$  are 1.33, 1.70, 2.14, 2.26,

2.14, and 1.70, respectively, centering at  $k'' = 1$ . A similar situation applies to  $W_n(\tau)$ , which is defined to be  $4\sigma_n(\tau)$ .

### 3.6. Mass patterns in Gaussian form

If the injected size is 1, and if  $k''$  value is not too large or too small ( $0.1 < k'' < 10$ ), the total mass patterns generated by the parcel matrix (in Fig. 5) can be approximated by a Gaussian equation:

$$m_t(n) = \frac{m_o}{\sqrt{2\pi\sigma_n(\tau)}} e^{-(n-n_p(\tau))^2/2\sigma_n(\tau)^2} \quad (25)$$

where the  $n_p(\tau)$  term is substituted by Eq. (22), and the  $\sigma_n(\tau)$  term is substituted by Eq. (24). The mass patterns for the stationary and mobile phases,  $m_s(n)$  and  $m_m(n)$ , synchronize with  $m_t(n)$  with the same position and standard deviation. They can be expressed in similar Gaussian equations after multiplying the corresponding mass fraction factors:

$$m_s(n) = \frac{k''}{k'' + 1} m_t(n) \quad (26)$$

$$m_m(n) = \frac{1}{k'' + 1} m_t(n) \quad (27)$$

Note that these equations should not be used when the sample size is larger than 1.

### 3.7. Mass peak heights

Since the peak area ( $A_n$ ) must be conservative,  $A_n \propto hW_n$  ( $h$  the peak height), the widest peak width occurs at  $k'' = 1$  which refers to the lowest peak height  $h$  for the total mass. The relationships between  $h_s$ ,  $h_m$ , and  $h_t$  (peak heights for the stationary, mobile phases and total sum, respectively) and  $k''$  values are shown in Fig. 7. The  $h_s(k'')$  and  $h_m(k'')$  curves cross at  $k'' = 1$ . If taking a logarithmic scale for  $k''$ , then the two curves are mirror images to each other centering at  $\log k'' = 0$ . If both axes are logarithmic, then the two curves appear like an “X” shape (between  $-1 < \log k'' < 1$ ), with slopes of 0.5 for  $\log h_s$  and  $-0.5$  for  $\log h_m$ .

Thus, the peak heights for the stationary and mobile mass patterns found on the parcel matrix (at a given  $\tau$ ) can also be estimated by:

$$h_s(\tau) \approx \frac{m_o}{\sqrt{2\pi(\tau + 0.5)}} \times \sqrt{k''} \quad (28)$$

$$h_m(\tau) \approx \frac{m_o}{\sqrt{2\pi(\tau + 0.5)}} \times \frac{1}{\sqrt{k''}} \quad (29)$$

where  $0.1 < k'' < 10$ .

### 3.8. Chromatographic peak shapes

As shown in Fig. 6, the chromatographic peaks generated by the matrix are all asymmetrical with a prolonged tail, no matter where the detector is located. Taking  $k'' = 1$  for instance, the mass distributions should be symmetrical at all time steps; but if viewed by the recorder, all peaks have a tail. In this case the tailing should be attributed exclusively to the temporal effect. If  $k'' \ll 1$ , the spatially non-asymmetrical profile (normal type) will be slightly more skewed, as both spatial and temporal tailing fractions synchronize. When  $k'' \gg 1$ , the spatial asymmetry is in the opposite direction to the temporal tailing, but it will be compensated by the latter. The resultant peak shape, although flat, still carries a normal type tail.

### 3.9. Temporal shift of peak position on $\tau$ coordinate

The appearance of a chromatographic peak summit on the time coordinate for a column length  $N$  is regarded as the retention time  $\tau_r$ . For example, when  $k'' = 1$  and  $n = 10$ , the peak summits were found at positions of  $P(1,1)$ ,  $P(2,2.5)$ ,  $P(3,4.5)$ ,  $P(10,18.5)$ ... etc., a  $1.5\tau$  unit ahead of the migration route. A general form is given:

$$\tau_r = \tau_{rm} - 0.5k'' \quad (30)$$

where the  $0.5k''$  term is named the “temporal shift”. Thus, the chromatographic peak would appear at the parcel position of  $n = N$  and  $\tau =$  “the nearest integer of  $(N - 0.5)(k'' + 1) - 0.5k''$  unless with a decimal of exactly 0.5 time units”. For example, when  $k'' = 0.5$  and  $n = 10$ , the chromatographic peak will be found at parcel  $P(10,14)$ ; when  $k'' = 5$  and  $n = 10$ , the peak summit will appear at  $P(10,54.5)$  instead of  $P(10,57)$  or  $P(10,60)$ .

The finding of the temporal shift is no surprise to

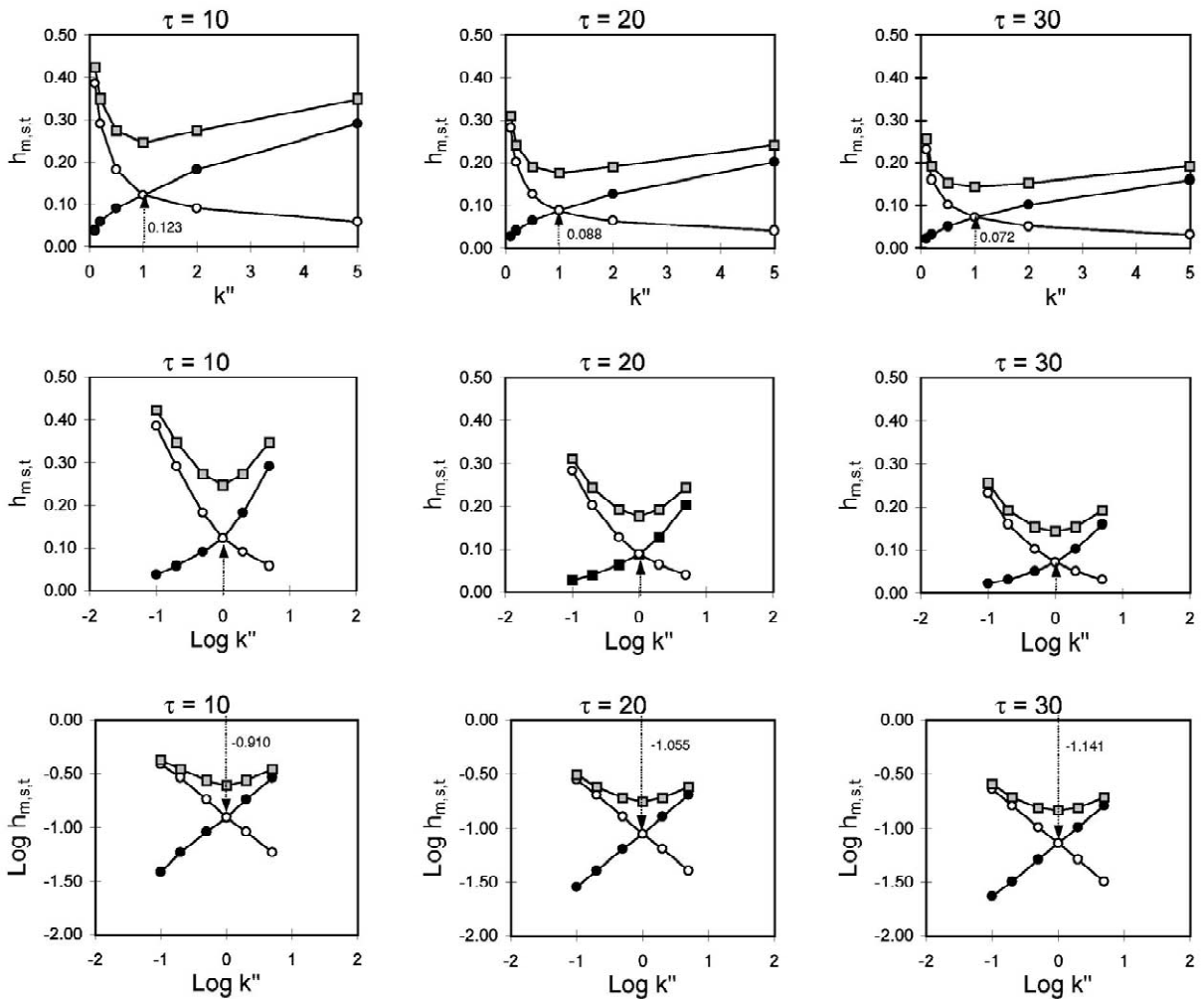


Fig. 7. Top, relationships between the mass peak height ( $h_m$ ) and partition ratio ( $k''$ ) at  $\tau=10, 20$  and  $30$ , respectively. Middle and bottom, logarithmic plots for  $h$  vs.  $\log k''$  and  $\log h$  vs.  $\log k''$  are also presented. The heights for the stationary phase ( $m_s$ ), mobile phase ( $m_m$ ) and total ( $m_t$ ) are marked with solid circle, open circle and cube, respectively. Arrows indicate the height data for  $h_m$  at  $k'' = 1$  or  $\log h_m$  at  $\log k'' = 0$ .

chromatography, as similar conclusions have already been demonstrated by Golshan-Shirazi and Guiochon [13] for at least three types of chromatographic models including: the plate or tank-in-series model, the statistical model, and the solutions of the partial differential equations for mass transfer kinetics along a column. In those theories the peaks generated all lean toward the left on the time coordinate, and the position of the observed peak summit appears slightly earlier than that expected for the mass center.

The temporal shift is independent of column

length (section number), therefore it should not be ignored under the linear conditions unless  $k''$  is nearly zero.

### 3.10. Zone width on $\tau$ coordinate

The chromatographic peak shows the mobile-phase mass fraction only. Since total peak area on  $\tau$  coordinate ( $A_\tau$ ) must be conservative ( $A_\tau = A_n = m_o$  on the parcel matrix), the chromatographic peak will appear flatter than does the mass profile. According

to Eq. (16), the standard deviation of a temporal peak should expand by a factor of  $k'' + 1$  during the axial transformation. For example, if  $k'' = 1$ , then  $\sigma_\tau(\tau_r) = 2\sigma_n(\tau_{rm})$ ;  $k'' = 5$ ,  $\sigma_\tau(\tau_r) = 6\sigma_n(\tau_{rm})$ .

### 3.11. Chromatographic peak in Gaussian form under linear isotherm

Like the mass patterns, chromatographic peaks generated by the parcel matrix (Fig. 6) can be approximated by a convoluted Gaussian function [10]. The convolution of Eq. (27) for a given column length  $n = N$  will lead to the following equation:

$$m_m(\tau) = \frac{m_o}{\sqrt{2\pi k''\tau}} e^{-[\tau - (N - 0.5)(k'' + 1)]^2 / 2k''\tau} \quad (31)$$

This equation is quite similar to that derived by de Levie [18]. Although the 0.5 term is not shown in his equation, he did mention in text that the addition of 0.5 gives a better approximation.

### 3.12. Chromatographic peak height

The chromatographic peak height  $h(\tau_r)$  may be slightly higher than the mass peak height  $h_m(\tau_{rm})$ , i.e. the mobile-phase mass value in  $P(N, \tau_r)$  may be slightly higher than that in  $P(N, \tau_{rm})$ . The difference, however, is rather small. The peak height that appears on the temporal coordinate can be estimated by the following equation:

$$h_\tau(N) \approx \frac{m_o}{\sqrt{2\pi\tau_{rm}}} \times \frac{1}{\sqrt{k''}} \quad (32)$$

where  $\tau_{rm} = (N - 0.5)(k'' + 1)$ .

### 3.13. Temporal distortion under linear isotherms

For a mass peak centering at a parcel position  $P(N, \tau_{rm})$ , one can compare the mobile mass peak shapes from both vertical and horizontal directions, after the longitudinal axis has been normalized to cope with the temporal scaling. Examples of the overlapped peak mappings are shown in Fig. 8. Three  $k''$  values (0.2, 1, and 2) were used to demonstrate three types of mass peaks (normal tailing, symmetrical, and reverse tailing). For a column length of  $N = 10$ , the

mass center arrives at the detector at  $\tau_{rm} = 11, 19$  and 29, respectively. Accordingly, parcels  $P(10, 11)$ ,  $P(10, 19)$  and  $P(10, 29)$  are chosen as the mapping centers. By re-plotting the mass profiles on a normalized coordinate, i.e. the  $(2N - n)(k'' + 1)$  axis, and overlapping it onto the temporal peak diagram on a normalized  $\tau - \tau_{rm}$  coordinate, the temporal distortion effect can be clearly identified.

For  $k'' = 0.2$ , the mass peak is initially asymmetrical. Although it has a comparative quick expanding rate but moves fast through the detector, the chromatographic response implies only a little temporal distortion of the spatial pattern. At  $k'' = 1$ , the mass profiles are all spatially symmetrical; and therefore the tailing is completely temporal. For  $k'' = 2$ , the mass peak is asymmetrical and tilting to the reverse direction. The temporal effect overwhelms the spatially fronting fraction, leading to an apparent normal-type tailing.

The peak mapping also indicates that the temporal effect is minimal when  $k''$  is small or the residence time is short; and it becomes dominant when  $k''$  is large or the residence time is long. However, in the latter case, the appearance of the peak on the recorder chart will be wide and flat, which might cause most analysts to think that it has become a Gaussian shape (actually it is not at all times). This probably explains why the temporal distortion effect has always been ignored.

### 3.14. The effect of sample size

As it has been described in textbooks [2], the increasing sample size will cause the peak height to be increased in an exponential trend, and a delay of the peak position occurs. The large-size injection can be interpreted as a summation of many small one-impulse peaks that overlap together, each having a small time lag. However, the resultant peak shape can hardly be expressed by a single equation.

The present parcel matrix model provides a convenient numerical approach for simulating the peak shapes for various sample sizes. To double the sample volume one only needs to input the same mass number ( $m_o$ ) into both  $P(0, 0)$  and  $P(0, 1)$  parcels. For larger sizes one can input a row of data along the parcel set  $P(0, 0), P(0, 1), P(0, 2) \dots$  and so forth. If the incoming sample is continuous, the mass

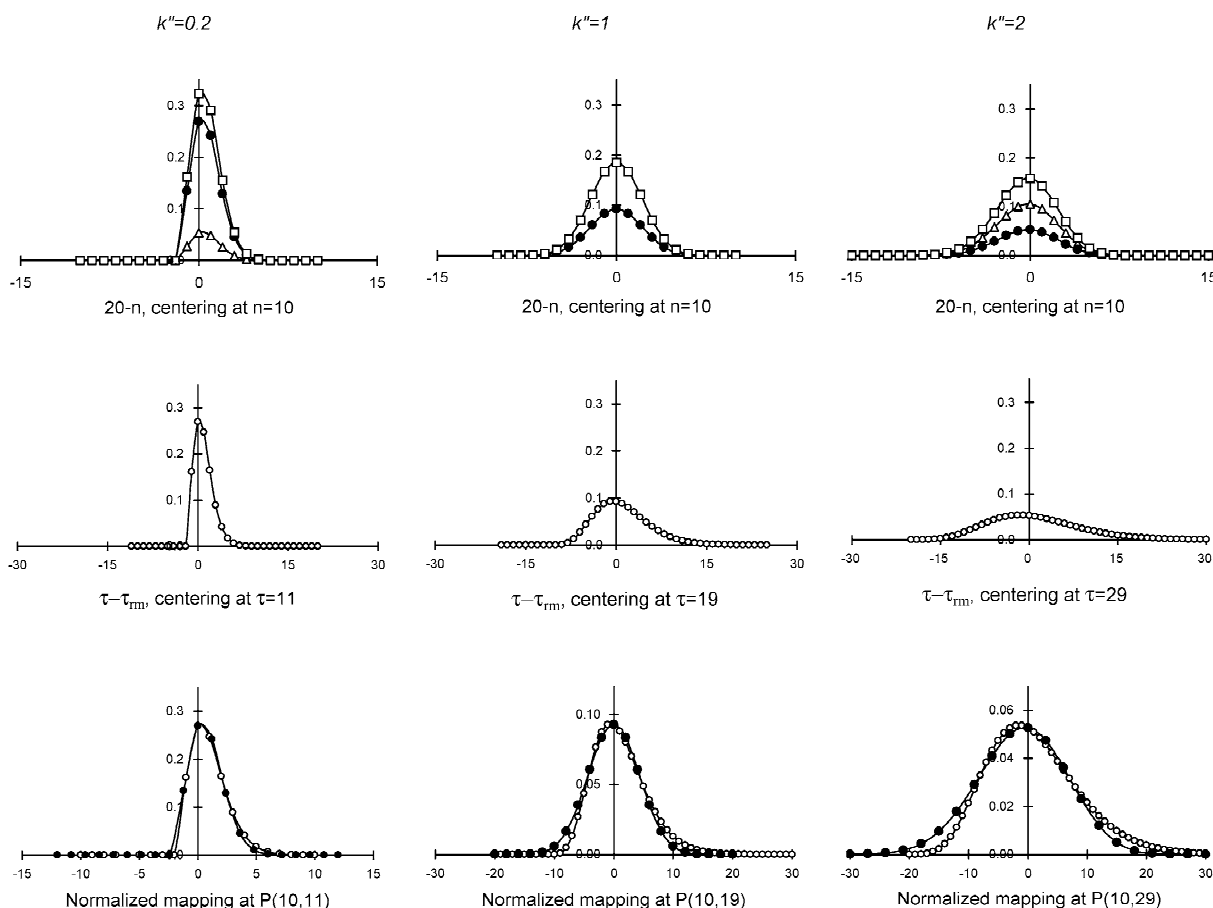


Fig. 8. Verification of the temporal distortion effect by overlapping spatial and temporal peaks under linear isotherms. Top, mass profiles plotted on  $2N - n$  coordinate for  $k'' = 0.2, 1$  and  $2$ , respectively, centering at  $n = 10$ . Stationary phase, open triangle; mobile phase, black circle; total mass, open square. Middle, chromatographic peaks on the  $\tau - \tau_{rm}$  coordinate for  $k'' = 0.2, 1$  and  $2$ , centering at  $\tau = 11, 19$  and  $29$ , respectively, marked with open circle. Bottom, normalized mapping plots on  $(20 - n)(k'' + 1)$  and  $\tau - \tau_{rm}$  coordinates. The difference between the two curves contributes to the temporal distortion effect.

can be filled from  $P(0,0)$  to infinite  $P(0,\tau)$ , the resultant chromatogram will become the “break-through curve” as can be seen in the frontal analysis.

Examples are given in Fig. 9. In this demonstration the mass and temporal peaks are plotted for five sample sizes ( $i = 1, 2, 5, 10$  and  $20$ , respectively). Three  $k''$  values ( $0.2, 1$  and  $2$ ) are used. The mobile-phase mass profiles are plotted at  $\tau = 20$ , and the temporal chromatographic peaks are plotted at a detecting position of  $n = 20$ .

In general, when  $k''$  is small, the increase of the sample size will give rise to a “plateau-like” sample zone; and when  $k''$  is large, the mass profile will maintain its peak shape, only it is fatter or wider (see

Fig. 9a–c). The mass peak position ( $n_p$ ) will have an apparent delay, this is because of the late entrance of the mass center (Fig. 9d). The migration speed  $\nu_m$  seems to be slower than expected in the starting period, but it will reach the normal speed when  $\tau$  is long enough, or after all sample sections have entered the column bed.

On the temporal coordinate, all chromatographic peaks are in “distorted mirror-images” to the mass patterns (see Fig. 9f–h). Accordingly, when the sample size is increased, the peak appearance time will have an extra delay (Fig. 9i). The peak heights are also increased depending on the injection size and  $k''$  value (Fig. 9j).

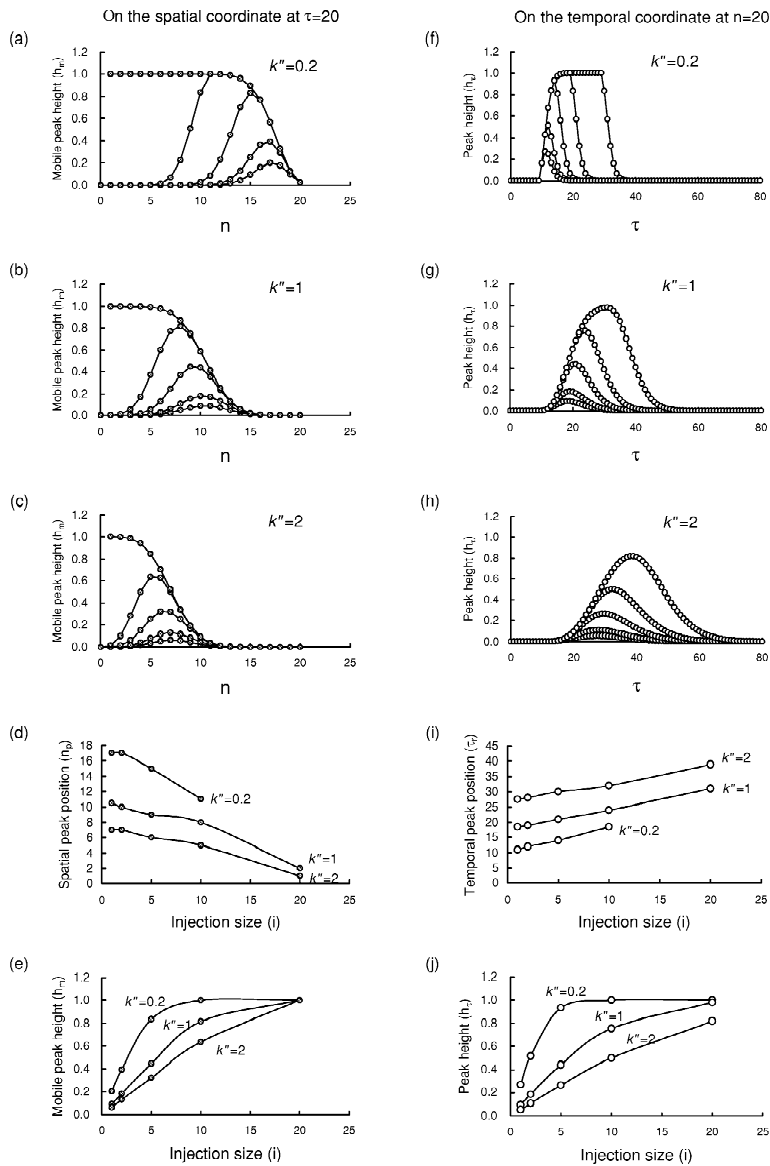


Fig. 9. Effects of changing injection sizes (injection sizes  $i = 1, 2, 5, 10$  and  $20$ , respectively) on the peak shape and parameters. Left, on the spatial coordinates; right, on the temporal coordinate. (a–c) Mobile-phase mass patterns for  $k'' = 0.2, 1$  and  $2$ , respectively, at time step  $\tau = 20$ . (d) Shift of the mass peak positions with the increase of the injection sizes,  $n_p$  vs.  $i$ . (e) Increase of the mass peak height with the increase of the injection sizes,  $h_m$  vs.  $i$ . (f–h) Chromatographic peak heights for  $k'' = 0.2, 1$  and  $2$ , respectively, as observed at  $n = 20$ . (i) Delay of the temporal peak position with the increase of the injection sizes,  $\tau_p$  vs.  $i$ . (j) Increase of the temporal peak height with the increase of the injection sizes,  $h_t$  vs.  $i$ .

#### 4. Numerical demonstration under non-linear isotherms

##### 4.1. Conditions of changing isotherms

Although the linear parcel matrix produces prom-

ising chromatographic peak shapes, its usefulness is quite limited. When  $k''$  is large, the retention time will be long, and the peak shape will appear to be very “flat”. Also, no fronting peak shape will be generated at any linear circumstance. Therefore it

cannot be applied to simulate the separation of a variety of components, or to compose a chromatogram as commonly seen in the laboratory.

However, it should be noted again that what can be observed on the recorder is just a distorted image, not the real spatial pattern. A “flat” chromatographic peak (on  $\tau$  coordinate) does not mean that the sample zone is “wide” in the column (on  $n$  coordinate). On the contrary, the bandwidth, although invisible to the detector, may still be narrow even if the time is quite long, only the migration speed is slow. If the isotherm can be changed ( $k''(\tau)$  value drops down), it is possible to release the mass from the stationary phase and to speed up the migration, thus giving a shaper chromatographic peak.

In practice, this can be done by elevating temperature (for GC), increasing the ionic strength or altering the polarity of the mobile solvent (for HPLC) [2,3]. In the present model, these conditions can be simulated by the programming of  $k''(\tau)$  values on a computer worksheet.

#### 4.2. Effects of changing $k''$ to peak parameters

The sudden change of the  $k''(\tau)$  value of a component during its migration in a column will promptly influence the migration route, the zone broadening and the final peak appearance. An example is demonstrated in Fig. 10. In this example, the in-

jection size and mass value are all 1, and the detector is placed at  $n=5$ . The initial  $k''_0$  value is 8, but changes to 0.8 at  $\tau=11$ . The impacts on the migration route, peak width and mass patterns are (as illustrated in Fig. 11) as follows.

1. The migration route turns downward; the  $\tau/n$  ratio changes from 9 to 1.8.
2. The expanding rate of the sample zone becomes larger after  $\tau=11$ , judging from the standard deviation or peak width.
3. The mass within a parcel re-distributes after the changing. For example, the mass ratio between the stationary and mobile phases is 8 before  $\tau=10$  and becomes 0.8 after  $\tau=11$ . In other words, a substantial fraction of mass is released from the stationary phase and appeared in the mobile phase. The migration speed is accelerated accordingly.
4. The appearance of the chromatographic peak is earlier with a much higher peak height compared to that if the  $k''(\tau)$  value was not changed.

#### 4.3. Temporal distortion when $k''(\tau)$ changes

A further verification of the “spatial tailing” or “temporal tailing” is made on a  $20 \times 60$  matrix (Fig. 12). In this demonstration a compound with an initial  $k''_0$  value of 8 is injected (the mass value is 1) into a column having a hypothetical detector placed at  $n=10$ .

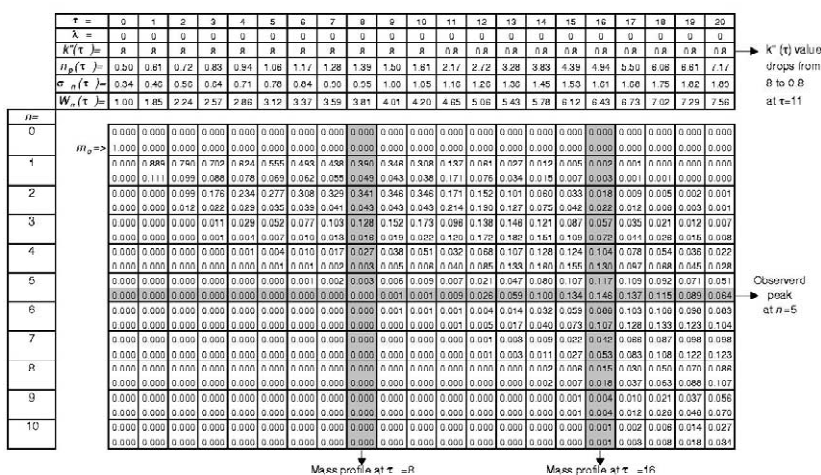


Fig. 10. A  $10 \times 20$  non-linear parcel matrix demonstrates the changing of the migration behaviors of a sample with an initial mass value of 1, and an initial  $k''_0 = 8$ , which changes from 8 to 0.8 after  $\tau=11$ . The vertical shaded data sets at  $\tau=8$  and 16 are plotted for the mass profiles, whereas the horizontal shaded data row at  $n=5$  is plotted for the chromatogram (shown in Fig. 11).

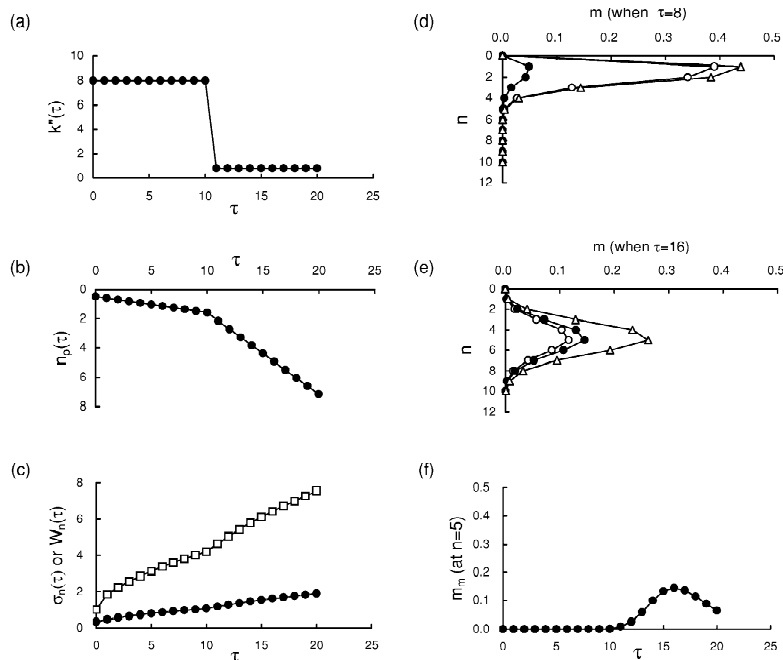


Fig. 11. Parameter plots for data generated by the parcel matrix in Fig. 10. (a) The  $k''(\tau)$  value changed from 8 to 0.8 when  $\tau=11$ . (b) The migration route turns downward with a  $\tau/n$  slope of  $k''(\tau) + 1$ . (c) Expanding of  $\sigma_n(\tau)$  and  $W_n(\tau)$  with time steps. (d) Mass profiles for the stationary (open circle), mobile (solid circle), and the total (triangle) phases when  $\tau=8$  (before the  $k''(\tau)$  change). The spatial distribution appears to be fronting. (e) Mass profiles when  $\tau=16$  after  $k''$  drops to 0.8. The spatial distribution turns out to be quite symmetrical. (f) Response recorded at  $n=5$ . The peak appears at  $\tau=16$  with a significant temporal tailing.

Under the linear isotherm, the migration speed ( $u_m(\tau)$ ) is slow, to be  $\Delta n_p(\tau)/\Delta\tau = v/(1+k''_o) = 0.111$ . The mass patterns (e.g. when  $\tau=20$ ) show a reverse type tailing, with one ninth of the total mass in the mobile phase and the rest (eight ninths) in the stationary phase. If the initial isotherm remains constant, then the mean residence time for the mass peak will be:  $\tau_{rm} = (10 - 0.5) \times (8 + 1) = 85.5$ ; the appearance of the peak on the temporal coordinate will be:  $\tau = \tau_{rm} - 0.5k'' = 81.5$ . The retention time would be too long to observe and the outcome peak shape will be very flat.

The changing of the isotherm is arranged at  $\tau=21$ , and the  $k''(\tau)$  value is dropped from 8 to 0.01, 0.2, 1 and 2, respectively. The sudden dropping of the  $k''(\tau)$  value alters the mass equilibrium between the stationary and mobile phases. The migration routes bend downward with  $\tau/n$  ratios of 1.01, 1.2, 2, and 3 (see Fig. 12, top left). The mass retention times are shortened to  $\tau_{rm} = 28, 29, 34.5$  and 42, respectively. The outcome peak shapes are quite different for the

four cases: fronting for  $k''(\tau) = 0.01$ , nearly symmetrical for  $k''(\tau) = 0.2$ , and with a prolonged tail for  $k''(\tau) = 1$  and 2 (see Fig. 12, top right). The temporal shifts ( $\tau_{rm} - \tau_r$ ) match exactly the scale of  $0.5k''(\tau_{rm})$ , as predicted.

The normalized overlapping of peaks (or residual analysis) at the detector position ( $n=10$ ) when the mass center arrives ( $\tau = \tau_{rm}$ ) provides the clue to distinguish the spatial and temporal effects. For the above four sets of peaks, the mapping centers were chosen at parcel positions of  $P(10,28)$ ,  $P(10,29)$ ,  $P(10,34)$  and  $P(10,42)$ . In Fig. 12, black circles mark the normalized mobile-phase patterns, whereas open circles mark the observed peaks.

Case 1  $k''(\tau)$  value drops from 8 to 0.01 at  $\tau=21$ , and the mass peak arrives at the detector at  $\tau=28$ . The total mass pattern at  $\tau=28$  remains almost the same fronting shape as that at  $\tau=20$ , but the mass fraction ratio for the stationary and mobile phases changes from 8:1 to 1:100. The mass pattern is

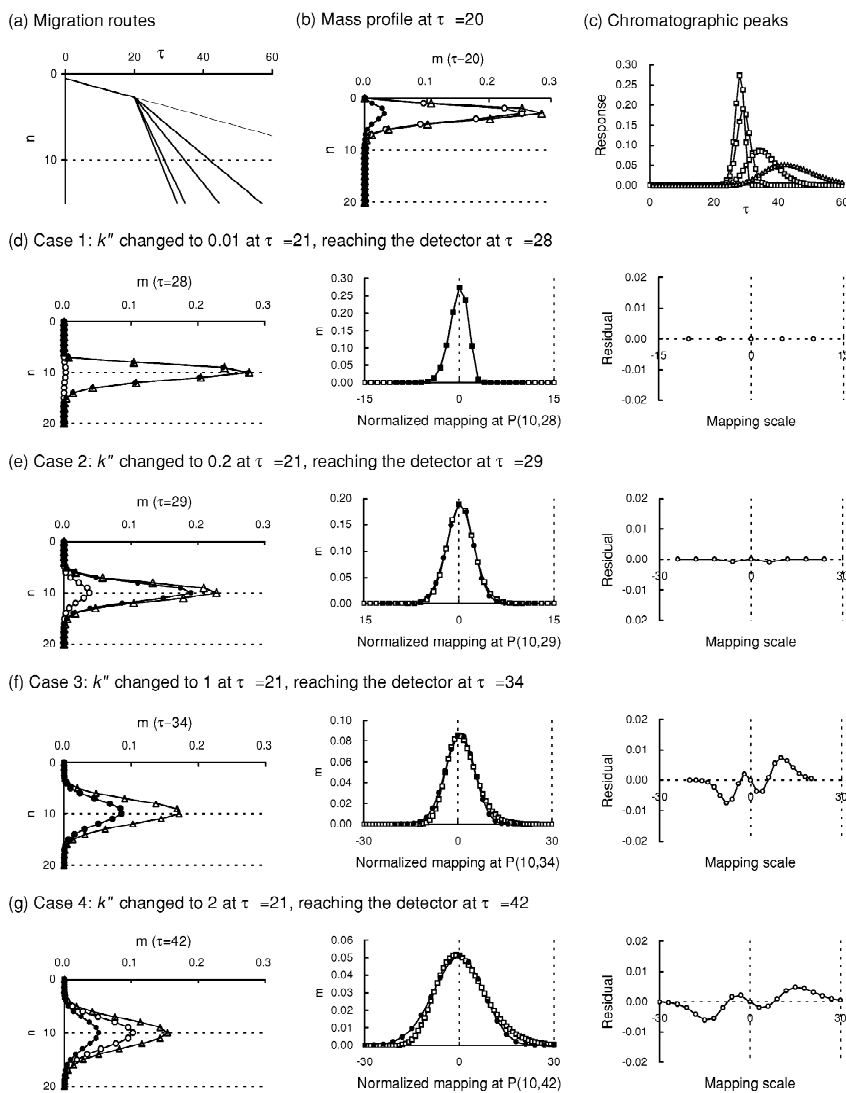


Fig. 12. Demonstration of how the “isotherm change” will affect the peak formation for a compound having an initial  $k''_o$  value of 8. (a) The migration routes on the  $n \times \tau$  matrix for a component if the  $k''_o$  value is changed from 8 to 0.01, 0.2, 1 and 2, respectively at  $\tau=21$ . (b) The mass profiles at  $\tau=20$  (before changing). Circle, dot and triangle represent the stationary, mobile and total mass patterns. (c) The resultant chromatographic peaks observed by a detector at  $n=10$ . (d) Case 1 ( $k''$  changed to 0.01): the mass profile at  $\tau=28$  is of a fronting-type; the mobile phase-pattern matches perfectly the temporal image (marked as open cube), leaving no temporal distortion residual. (e) Case 2 ( $k''$  changed to 0.2): the mass profile at  $\tau=29$  is still fronting; but is slightly less fronting for the temporal image. A very small residual can be seen. (f) Case 3 ( $k''$  changed to 1): the mass profile at  $\tau=34$  becomes quite symmetrical, but the temporal image carries a tail. The temporal distortion is identified by the residual plot. (g) Case 4 ( $k''$  change to 2): the mass profile at  $\tau=42$  is nearly Gaussian, and the temporal tailing becomes obvious.

almost identical to the chromatographic peak, and the residual analysis shows that there is almost no temporal distortion. The skewness of the chromatographic peak

(fronting-type) can be considered exclusively “spatial”.

Case 2  $k''(\tau)$  drops to 0.2 and the mass center arrives at  $\tau=29$ . The mass pattern is slightly

fronting and the height is lower than it is in case 1. The fraction between the stationary and mobile phases is 1:5. When it is overlapped on the chromatographic peak, a very small residual can be seen. This temporal distortion compensates for the spatial fronting fraction and the resultant outlook is quite symmetrical.

Case 3  $k''(\tau)$  drops to 1 and the mass center arrives at  $\tau=34.5$ . Since the parcel addresses are all integers, the data column at  $\tau=34$  is plotted. The mass pattern turns out to be quite symmetrical after the travel period between  $\tau=21$  and 34. The mass ratio between the stationary and mobile phases is 1:1, and the  $\tau/n$  ratio is 2. The recorder gives an obvious normal-type tailing. The temporal distortion is identified by the residual curve analysis.

Case 4  $k''(\tau)$  drops to 2 and the mass center arrives at  $\tau=42$ . The mass profiles are nearly Gaussian, but viewed by the recorder to have a tail. At a  $\tau/n$  ratio of 3, the temporal distortion becomes even more obvious in proportion. In contrast to case 1, the skewness of the chromatographic peak (prolonged tailing) may be considered exclusively “temporal”.

The shape of the residual curves for the latter two cases (twisted like an earthworm) is very similar to that previously reported for flow injection analysis [10]. It has three crossing knots on the horizontal coordinate, which means that at least three points of the observed peak can be free from the temporal distortion. However, it should be noted that the expansion forces for the two techniques are different. In the present model the expanding is induced only by the retention behavior in the column, whereas for FIA it is generated by diffusion. Nonetheless, the resultant phenomena are similar.

#### 4.4. Simulating the temperature programming

In gas chromatography, the most effective way to reduce the apparent partition ratio would be the increase of temperature. In general, the relationship between the  $k''(\tau)$  value and temperature can be

described as:  $\log k''(\tau) \propto 1/T$ . For simplicity, the relationship is assumed the same for all components. The setting of a program for the temperature elevation can be stage-wise, continuous, or first a continuous rising then a terminal stage to release those highly retarding compounds from the column.

Examples are given in Fig. 13 for four different components with initial dynamic partition ratios  $k''_0$  of 1, 5, 10 and 50, respectively. If these ratios were kept unchanged throughout the operation, then only one peak ( $k''_0 = 1$ ) could be observed ( $\tau_{rm} = 39$ ) for a column (length=20) within the 100 time-step duration.

When the temperature is changed twice (Fig. 13a) at  $\tau=20$  and 40, and  $k''(\tau)$  values are dropped to be 1/2 and 1/4 of the initial  $k''_0$ , the  $\tau/n$  slopes of the migration routes for the four components change from the initial 2, 6, 11 and 51 to 1, 3, 5.5 and 25.5; then 0.5, 1.5, 2.75 and 12.25, respectively. The peaks are sharper in shape, appear earlier, and all carry a normal-type tailing. A little hump is noticed at the trailing edge of the first peak, marking the changing point at  $\tau=40$ .

In the case of Fig. 13b, since the  $k''(\tau)$  values are changed continuously at a decay rate of  $\lambda=0.05$  (Eq. (13)), the mass migration routes become concave curves. The final  $k''(\tau)$  values when arriving at the detector ( $n=20$ ) are 0.23, 0.45, 0.52 and 0.58, respectively. The corresponding  $\tau/n$  ratios become 1.23, 1.45, 1.52 and 1.58. These slope values are much lower and lead to higher peak heights and sharper looks. Also, the effect of temporal distortion is less significant and therefore all peaks look quite symmetrical.

In many circumstances a terminal high temperature is applied to rush out those high  $k''_0$  value compounds that are still bound to the column. A simulation is given in Fig. 13c, in which the  $k''(\tau)$  value is initially decreased at a decay rate of 0.05 and then suddenly dropped to 1/100 and maintained hereafter at  $\tau=50$ . This sudden change will not affect the first peak which has already passed through the detector, but will accelerate the migration speeds of those that still are retained in the column. It is noted that the second peak has a double-summit, one before the drastic temperature change and one after. It gives the peak a blunt rising edge and a sharp trailing edge, and thus can be

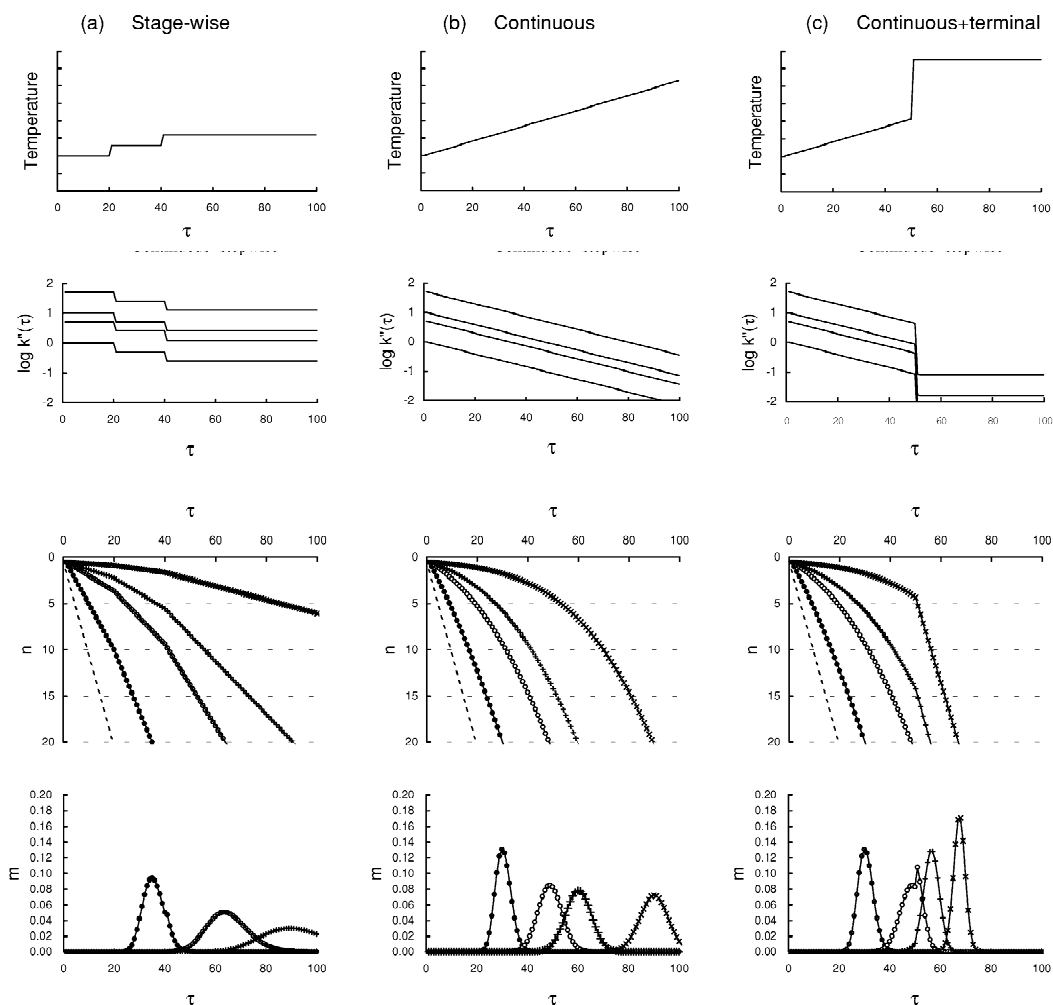


Fig. 13. Temperature programming and how it affects the  $k''(\tau)$  values, migration routes and resultant peak shapes in gas chromatography. Top row, the temperature is programmed to be (a) stage-wise increasing, (b) continuous increasing, and (c) continuous plus a terminal increasing. 2nd row, the change of  $k''(\tau)$  for the four components with initial  $k''_0$  values of 1, 5, 10 and 50, respectively. 3rd row, the mass migration routes for the four components under various isotherms. Dashed line denotes the void position. Bottom row, the chromatogram obtained at  $n=20$ . Note that at the changing points some spikes might occur on the peak shoulder.

regarded as a temporal fronting-type peak. The third peak, with an initial  $k''_0 = 10$ , ends with a  $k''(\tau_{rm})$  value of merely 0.016 or a  $\tau/n$  slope of 1.016 when it passes through the detector. The migration speed ( $v_m = 1/1.016v$ ) reaches 98.4% of the flow speed of the mobile solvent. At this speed the temporal distortion is almost diminished, and the observed peak shape is almost identical to the spatial pattern, to be very symmetrical. The same situations apply to

the last peak (initial  $k''_0 = 50$ ), which ends at a  $\tau/n$  ratio of 1.08, giving a nearly Gaussian type peak.

It is interesting to note that all 11 peaks shown in Fig. 13 are almost Gaussian in the spatial domain when arriving at the detector, regardless of the change of the isotherm during the migration. Therefore, the peak tailing, fronting, and even the doublet are all spatially “false”, as a result of the temporal distortion effect.

4.5. Equations for migration routes under non-linear isotherms

Although the mass peak position can be calculated by Eq. (18) in a recursion manner on the parcel matrix, it can also be expressed by migration route equations depending on the conditions of  $k''(\tau)$  programming.

(a) When  $k''(\tau)$  is changed in a stage-wise manner.

If the changing of  $k''(\tau)$  is made stage-wise with  $j$  stages, and changing at  $\tau_j$ , the position of the mass peak on the  $n$  coordinate will be:

$$n_p(\tau) = 0.5 + \frac{1}{k''_1 + 1}(\tau_1) + \frac{1}{k''_2 + 1}(\tau_2 - \tau_1) + \dots \tag{33}$$

Accordingly, the general formula for programming with  $j$  stages each has a  $k''_j$  value of:

$$n_p(\tau) = 0.5 + \sum_{j=1}^j \left( \frac{(\tau_j - \tau_{j-1})}{k''_j + 1} \right) \tag{34}$$

(b) When  $k''(\tau)$  is decreased following Eq. (12).

If the changing of  $k''(\tau)$  values follows  $k''(\tau) = k''_0(1 - \lambda\tau)$ , the migration route will be:

$$n_p(\tau) = 0.5 + \int_0^\tau \frac{1}{k''_0(1 - \lambda\tau) + 1} d\tau \tag{35}$$

or

$$n_p(\tau) = 0.5 - \frac{1}{\lambda k''_0} \ln(k''_0 - \lambda k''_0 \tau + 1) + \frac{1}{\lambda k''_0} \ln(k''_0 + 1) \tag{36}$$

(c) When  $k''(\tau)$  is decreased following Eq. (13).

If the changing of  $k''$  value is decreased exponentially ( $dk''/d\tau = -\lambda$ ), the mass peak position can be predicted approximately by the following equation:

$$n_p(\tau) = 0.5 + \int_0^\tau \frac{1}{k''_0 e^{-\lambda\tau} + 1} d\tau \tag{37}$$

or,

$$n_p(\tau) = 0.5 + \tau + \frac{1}{\lambda} \ln(k''_0 e^{-\lambda\tau} + 1) - \frac{1}{\lambda} \ln(k''_0 + 1) \tag{38}$$

The migration routes made by the above equation agree quite well with that obtained from the parcel matrix, with very small deviations even when  $\tau$  is small (see Fig. 14).

4.6. Equations for zone width under non-linear isotherms

The recursion calculation of the spatial zone width (or standard deviation of a peak) as stated by Eq. (15) can also be expressed as equations.

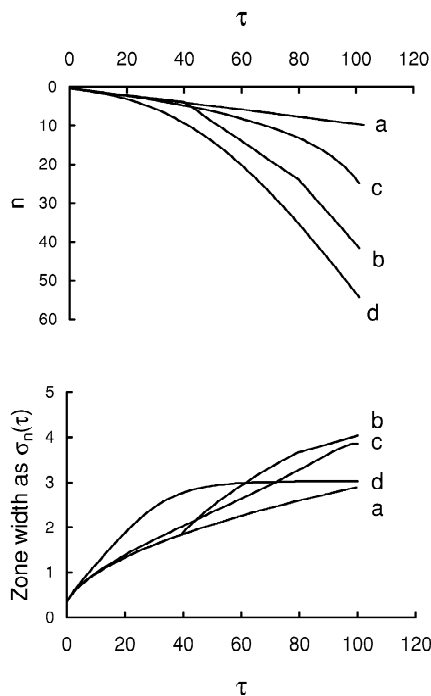


Fig. 14. Examples of using equations to predict (top) the migration route, i.e. Eqs. (22), (34), (36), (38), and (bottom) the zone broadening, i.e. Eqs. (24), (40), (42), (45), under various isotherms. The initial  $k''_0$  values are 10 for all cases. The conditions for the  $k''(\tau)$  programming are: (a) constant throughout, (b)  $k''(\tau)$  is changed from 10 to 1 at  $\tau=40$  and to 0.2 at  $\tau=80$ , (c)  $k''(\tau)$  is decreased with a linear decay constant  $\lambda=0.1$ , (d)  $k''(\tau)$  is decreased with an exponential decay constant  $\lambda=0.1$ .

(a) When  $k''(\tau)$  is changed in a stage-wise manner.

If the initial  $k''_o$  value is changed in  $j$  stages during the migration (at  $\tau_1, \tau_2 \dots$  each has a  $k''_j$ ), the resultant standard deviation will be accounted for by:

$$\sigma_n(\tau)^2 = \sigma_o^2 + \frac{k''_o}{(k''_o + 1)^2} \tau_1 + \frac{k''_1}{(k''_1 + 1)^2} (\tau_2 - \tau_1) + \dots \quad (39)$$

or,

$$\sigma_n(\tau)^2 = \sigma_o^2 + \sum_{j=1}^j \frac{k''_{j-1}}{(k''_{j-1} + 1)^2} (\tau_j - \tau_{j-1}) \quad (40)$$

(b) When  $k''(\tau)$  is decreased following Eq. (12).

If  $k''(\tau)$  is programmed to be decreasing continuously in a linear trend with  $\tau$ , i.e.  $k''(\tau) = k''_o(1 - \lambda\tau)$  and  $0 \leq \lambda\tau \leq 1$ :

$$\sigma_n(\tau)^2 = \sigma_o^2 + \int_0^\tau \frac{k''_o(1 - \lambda\tau)}{(k''_o(1 - \lambda\tau) + 1)^2} d\tau \quad (41)$$

then,

$$\sigma_n(\tau)^2 = \sigma_o^2 - \frac{1}{\lambda k''_o} \left[ \ln(k''_o - \lambda k''_o \tau + 1) + \frac{1}{k''_o - \lambda k''_o \tau + 1} \right] + \frac{1}{\lambda k''_o} \left[ \ln(k''_o + 1) + \frac{1}{k''_o + 1} \right] \quad (42)$$

(c) When  $k''(\tau)$  is decreased following Eq. (13).

If  $k''(\tau)$  is programmed to be decreasing continuously in an exponential trend, i.e.  $k''(\tau) = k''_o e^{-\lambda\tau}$ , then:

$$\sigma_n(\tau)^2 = \sigma_o^2 + \int_0^\tau \frac{k''_o e^{-\lambda\tau}}{(k''_o e^{-\lambda\tau} + 1)^2} d\tau \quad (43)$$

The solution for this integration will be:

$$\sigma_n(\tau)^2 = \sigma_o^2 + \frac{1}{\lambda} (k''_o e^{-\lambda\tau} + 1)^{-1} - \frac{1}{\lambda} (k''_o + 1)^{-1} \quad (44)$$

or,

$$\sigma_n(\tau) = \sqrt{\sigma_o^2 + \frac{1}{\lambda(k''_o e^{-\lambda\tau} + 1)} - \frac{1}{\lambda(k''_o + 1)}} \quad (45)$$

When  $\tau$  is large enough or the  $e^{-\lambda\tau}$  term approaches zero, the band width will no longer expand and will converge to the square root of the initial variance plus a boundary of  $[k''_o/(k''_o + 1)]/\lambda$ . Under this circumstance, all, except the leading peaks (on  $\tau$  coordinate), will be almost identical with the same zone width (see Fig. 14d).

#### 4.7. Position of chromatographic peaks

Under non-linear isotherms, the time for the mass peak to migrate to the end of a column of length  $N$  ( $\tau_{rm}$ ) is quite difficult to calculate directly by a single equation (e.g. solving Eqs. (34), (36) or (38) for  $\tau_{rm}$  when  $n_p(\tau_{rm}) = N$ ), but it can be estimated graphically on the matrix. The time for the appearance of the chromatographic peak on  $\tau$  coordinate ( $\tau_r$ ) is then calculated by  $\tau_{rm} - 0.5k''(\tau_{rm})$ . In most non-linear cases it can be neglected because the final  $k''(\tau_{rm})$  is dropped to almost zero when arriving at the detecting point.

#### 4.8. Peak width on $\tau$ coordinate

Like under the linear isotherms the standard deviation of a chromatographic peak for a column length of  $N$  is accounted for by:  $\sigma_\tau(\tau_{rm}) = (k''(\tau_{rm}) + 1)\sigma_n(\tau_{rm})$ . The peak width  $W_\tau(\tau_{rm})$  equals  $4\sigma_\tau(\tau_{rm})$ . Under non-linear isotherms, the extent of peak distortion is dependent on the zone broadening rate, i.e.  $\Delta\sigma_n(\tau_{rm})/\Delta\tau$ . Therefore when the final  $k''(\tau_{rm})$  drops to near zero, the temporal distortion effect can be very small. However, since  $k''(\tau)$  is still decreasing before and after arriving at the detector, a small fronting distortion will still occur.

#### 4.9. Asymmetry transformation on a chromatogram

In separating a group of compounds, the chromatogram may comprise of many peaks with various shapes. The leading peaks usually appear with prolonged tails, which are followed by several groups of peaks. Some are fronting, while others

have irregular shapes or doublets, and some are nearly symmetrical. In the terminal stage, the last peaks may have significant fronting tails, which sometimes exhibit even narrower peak widths and higher heights. When these happen, it would be very puzzling for analysts to explain why and how the peak asymmetry is transformed from “tailing” to “fronting”.

With the aid of the  $k''(\tau)$  programming, it is possible to create such patterns on the parcel matrix. Firstly, the peak shape of each component is generated individually; then, all peaks are overlapped or combined to compose a complete chromatogram.

An example is given in Fig. 15. A short column ( $N=10$ ) is used to separate a group of 18 components assumed to have initial  $k''_0$  values of 0.2, 0.5, 1, 1.5, 2, 3, 5, 10, 20, 50, 100, 300, 500, 1000, 3000, 5000, 10 000 and 30 000, respectively. The isotherm has been programmed in three stages: (1)  $\tau=0-50$ , all  $k''(\tau)$  are constant; (2)  $\tau=51-200$ , all  $k''(\tau)$

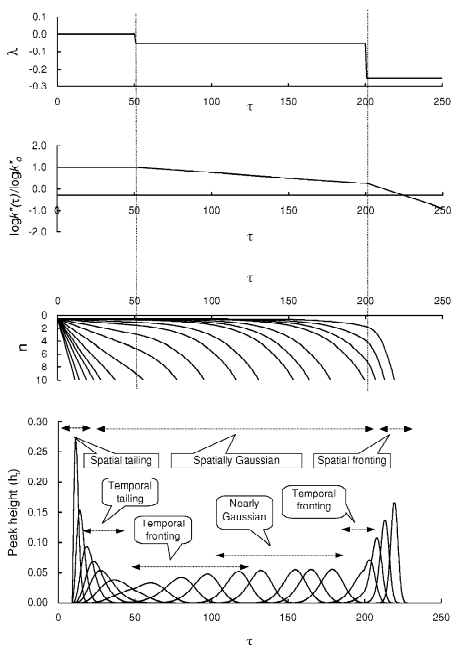


Fig. 15. Transformation of peak asymmetry on a chromatogram as illustrated by a non-linear  $10 \times 250$  parcel matrix programmed to have three-stage isotherms. The exponential decay constant ( $\lambda$ ) is 0 during  $\tau=0-50$ , changes to 0.05 during  $\tau=51-200$ , then 0.25 after  $\tau=201$ . Eighteen components are demonstrated with initial  $k''_0$  values of 0.2, 0.5, 1, 1.5, 2, 3, 5, 10, 20, 50, 100, 300, 500, 1000, 3000, 5000, 10 000 and 30 000, respectively.

decrease exponentially at a decay rate  $\lambda=0.05$ ; (3) after  $\tau=201$ ,  $\lambda$  becomes 0.25.

In the linear stage ( $\tau=0-50$ ), the leading peaks appear with prolonged tails as expected. By comparing the spatial patterns with chromatographic peaks, it is proven that the spatially-induced tailing fraction is large at the beginning but gradually decreasing with time; whereas the temporally-induced tailing fraction is small at the beginning, but is gradually increasing. At  $\tau=51$  when the isotherm has been changed, the spatial patterns in the column maintain a Gaussian shape, but the temporal peak shape transforms from tailing to fronting. When the exponential isotherm becomes stable, the peaks that appear during  $\tau=100-200$  are all identical in shape, width and height, with a very slight temporal fronting (so small that they all look like Gaussian curves). Near the second changing point ( $\tau=201$ ), the temporally-induced fronting effect occurs again, then fades rapidly. In the terminal stage, the peaks appear with slight fronting, which is mainly due to the retardation of those high  $k''_0$  components. The temporal distortion effect becomes negligible at the end of the chromatogram as the final  $k''(\tau)$  values are very small.

The fronting caused by the temporal distortion effect may be small under “stable” non-linear isotherms, but can be very obvious near the drastic changing points.

#### 4.10. Graphical display of the asymmetrical fractions

The peak asymmetry can be expressed by dividing the peak width into two sections at the rising and trailing sides of a peak (Fig. 16). For example, on the longitudinal coordinate,  $W_n = a + b$ . The mass pattern is symmetrical when  $a$  equals  $b$ ; and vice versa. Similarly, the width of a chromatographic peak can be expressed as  $W_\tau = a' + b'$ . The peak shape is symmetrical when  $a' = b'$ , has a prolonged tail when  $a' < b'$ , and is fronting when  $a' > b'$ . The contribution of the spatial and temporal tailing fractions can be identified by comparing the  $a, b, a'$  and  $b'$  sections along the migration route at a given column length  $N$  (marked by a horizontal dashed line in Fig. 16).

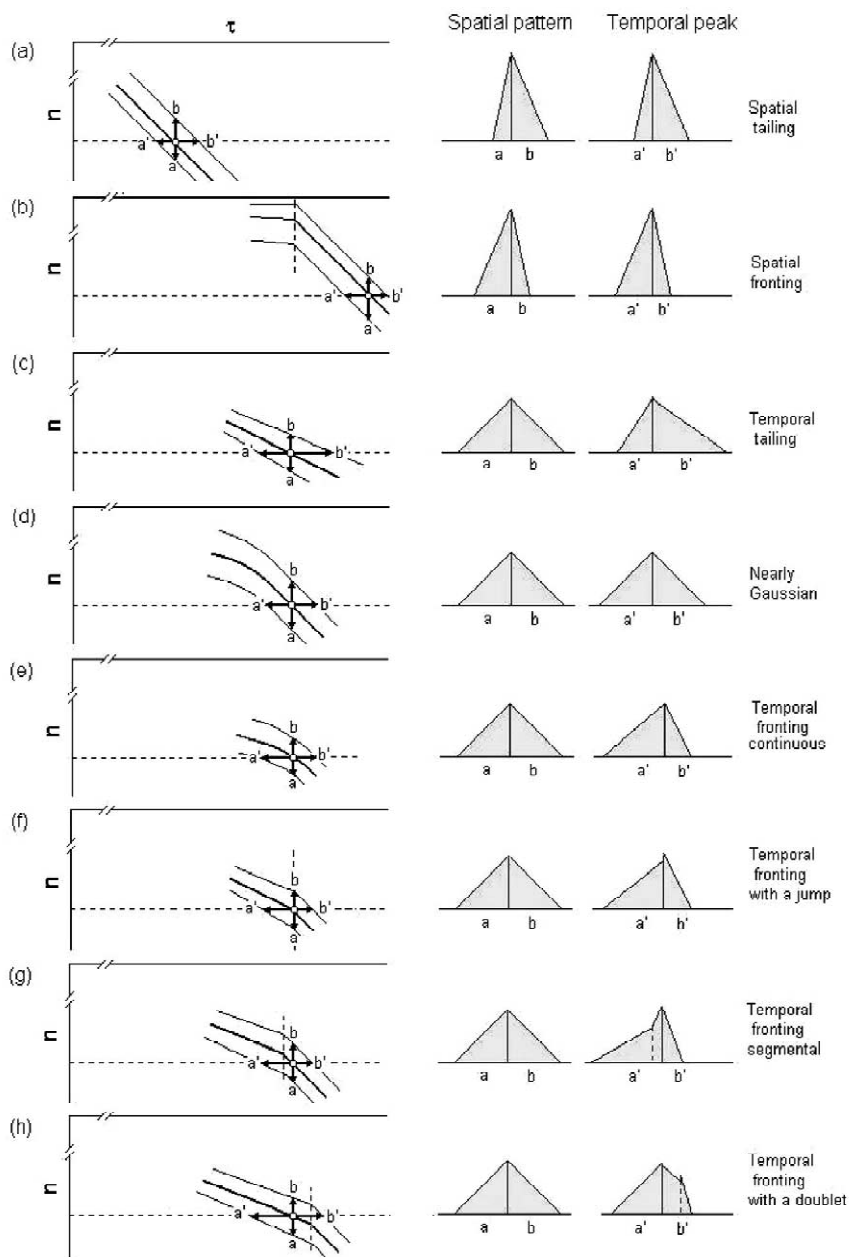


Fig. 16. Basic peak shapes that were generated by the parcel matrix. The peak widths on  $n$  and  $\tau$  coordinates ( $W_n$  and  $W_\tau$ ) are divided into the leading and trailing sectors, i.e.  $W_n = a + b$  and  $W_\tau = a' + b'$ . The migration routes and zone boundaries are shown on the left, whereas the mass patterns and resultant chromatographic peaks are shown on the right. Conditions for the eight cases (a)–(h), refer to text.

In general, eight basic types of peaks can be identified by the parcel matrix model. Only two types are related to the spatial reasons, whereas the rest are all induced by the temporal distortion effect.

(a) If the initial  $k''_0$  is very small, the mass peak has a sharp rising edge and a prolonged trailing edge ( $a < b$ ). When it arrives at the detector, the projected temporal image maintains a similar

pattern, i.e.  $a' < b'$ ,  $k''(\tau_{\text{rm}}) \approx 0$ ,  $a' \approx a$  and  $b' \approx b$ . The temporal distortion is insignificant.

- (b) If the initial  $k''_0$  is very large, the mass peak will have a blunt rising edge and a sharp trailing edge ( $a > b$ ). It migrates slowly in the column and will appear in the terminal stage when the  $k''_0$  value is dropped suddenly to almost zero (marked by a vertical dashed line in Fig. 16). In this circumstance, the migration slope turns to 1:1, and the temporal image reflects the real spatial asymmetrical pattern. Thus,  $a' > b'$ ,  $k''(\tau_{\text{rm}}) \approx 0$ ,  $a' \approx a$  and  $b' \approx b$ , a spatial fronting tail without any temporal distortion.
- (c) Under linear isotherms the migration route is linear, and the mass pattern is kept symmetrical ( $a = b$ ). While arriving at the detector, the temporal image is skewed ( $a' < b'$ ). This asymmetry occurs as an expanding of the peak width on both edges are in different slopes. The peak width expands following  $W_\tau = W_n(k'' + 1)$ ; whereas  $a'$  is slightly smaller than  $a(k'' + 1)$ ;  $b''$  is slightly larger than  $b(k'' + 1)$ , and a small temporal shift of peak position occurs.
- (d) Under non-linear isotherms, when high  $k''(\tau)$  value is decreased gradually to almost zero at the detection point. Spatially  $a = b$ ; temporally  $a' = b'$ . Since  $k''(\tau_{\text{rm}}) \approx 0$ ,  $a' \approx a$ ,  $b' \approx b$ , the peak appears like a Gaussian curve and the temporal distortion is minimal.
- (e) Same as above, the  $k''(\tau)$  value is dropping continuously but not so low as to reach zero. On the spatial coordinate the sample zone is Gaussian, but on the temporal coordinate it has a fronting shape, i.e.  $a = b$ ;  $a' > b'$ .
- (f) Under linear or non-linear isotherms, when  $k''(\tau_{\text{rm}})$  is not zero, but a sudden change of isotherm takes place when half of the sample zone has passed through the detector, i.e. the changing point is at  $\tau_{\text{rm}}$ . At the peak summit,  $a$  still equals  $b$ , but  $a'$  is larger than  $b'$ . A fronting peak appears. It should be noted that the stationary phase mass will be released to mobile phase, leading to a peak jump at  $\tau_{\text{rm}}$ .
- (g) Similar to case (f), but the changing point is slightly before  $\tau_{\text{rm}}$ . The peak shape is still fronting ( $a' > b'$ ), and it appears like the combination of two different peak segments.
- (h) Similar to case (f), but the changing point is

after  $\tau_{\text{rm}}$ . The peak is fronting and a doublet may occur.

In a real situation, the spatial and temporal asymmetry fractions may co-exist (also see the example in Fig. 15). A peak observed can be more skewed or less skewed depending on the location of the observation and how the final  $k''(\tau)$  or slope becomes when arriving at the detecting point.

#### 4.11. Approximation by Gaussian equations under non-linear isotherms

Apart from the type (a) and (b) peaks shown in Fig. 16, all other types of peak are spatially symmetrical. Thus, the total mass pattern can be approximated by the same Gaussian equation as shown in Section 3.6, i.e. Eq. (25). To do this, the term  $n_p(\tau)$  in Eq. (25) should be replaced by either one of Eqs. (34), (36), or (38); the term  $\sigma_n(\tau)$  should also be substituted by corresponding Eqs. (40), (42) or (45). The equation for the mobile-phase mass pattern is obtained by further multiplying by a factor of  $1/(k''(\tau_{\text{rm}}) + 1)$ . The value for  $k''(\tau_{\text{rm}})$  can be obtained either from the matrix or from Eq. (12) or (13). Although the final equation may become very large and complicated, it can still be displayed in a step-by-step manner on the computer spreadsheet.

For a chromatographic peak, the equation for the mobile-phase mass pattern (Eq. (27)) is further treated by a convolution process [10]. This temporally convoluted equation,  $m_m(\tau)$ , which is still in a Gaussian form, can generate all the temporally-induced asymmetrical peaks as shown in Fig. 15.

#### 4.12. Comparison with previous studies

The general reasons for the peak asymmetry found in Section 4.10 are quite different from those described in textbooks [2,8]. In the past, the non-linear isotherms were thought to be mainly responsible for the skewness. Thus, Langmuir type isotherms will lead to a normal-type peak tailing, whereas anti-Langmuir type isotherms will cause a reverse-type or peak fronting. However, using the parcel matrix model, normal-type peak tailings can occur under a linear isotherm, not necessarily only for the Langmuir type. Also, fronting peaks can be generated

under a non-linear or Langmuir isotherm, not necessarily only when using an anti-Langmuir type.

For solving and simulating asymmetrical peaks, many analysts favor the use of an exponentially modified Gaussian function (EMG) [5]. However, the concept of EMG is established on the assumption that the variance is in proportion to the travel distance or retention time. This is correct on the spatial coordinate, but irrelevant for the temporal appearance. Therefore the EMG functions can be used to simulate mass distribution profiles rather than chromatography peaks. A recent paper by Li [7], who compared the peak shapes derived from several improved EMG functions with real chromatographic peaks, gives a good clue concerning the peak asymmetry. The residual curves, plotted for the difference between the theoretical and experimental peaks, are all earthworm-like, very similar to those seen in Fig. 12 for the temporal deformation fraction.

A recent textbook by Lin and Guiochon [20] provides additional explanations on the peak asymmetry. They clearly state that the solution in linear chromatography is Gaussian only in an ideal case of a “Dirac” injection in space domain, which is based on an unrealistic assumption that the injection speed is infinitely fast. The authors suggest that a chromatographic peak may never be observed as a Gaussian curve. This is in good agreement with the findings of the present work.

## 5. Conclusion

The proposed parcel matrix model has successfully generated various asymmetrical peak shapes under linear and non-linear isotherms. It has improved Glueckauf's [16] dynamic model, Fritz and Scott's statistic model [17], and de Levie's linear worksheet models [18], leading to a more realistic simulation to the peak shapes that are commonly seen in the laboratory.

Although the present model might not solve all peak problems, it does indicate that the long-ignored temporal distortion effect can be the dominating reason for the peak asymmetry. The sample size is no longer limited to a single impulse, and the same parcel matrix can be used to perform pre-concentration or frontal analysis for a large volume sample.

With the aid of a computer spreadsheet (e.g. Microsoft Excel), the performance of the parcel model becomes very easy. Students benefit by learning the chromatographic behaviors and peak formations without prior knowledge of the van Deemter or diffusion equations. The author strongly suggests that this might be an alternative method for chromatography education.

## Acknowledgements

The author would like to sincerely thank L.S. Wen, C.S. Chern, L.Y. Chiao, Y.H. Li, G.T.F. Wong, C.W. Whang and K. Ronning for their kind assistance and discussion during the preparation of the manuscript. Suggestions by G. Guiochon and two anonymous reviewers are also gratefully appreciated. This project is partially sponsored by the National Science Council (Taipei) under grant no. NSC91-2611-M-002-009.

## References

- [1] D.A. Skoog, F.J. Holler, T.A. Nieman, in: 5th ed, Principles of Instrumental Analysis, Saunders College, Philadelphia, 1998.
- [2] K. Robards, P.R. Haddad, P.E. Jackson, Principles and Practice of Modern Chromatographic Methods, Academic Press, London, 1994.
- [3] D.C. Harris, in: 4th ed, Quantitative Chemical Analysis, W.H. Freeman, 1995.
- [4] J.P. Foley, J.G. Dorsey, *J. Chromatogr. Sci.* 22 (1984) 40.
- [5] J.P. Foley, *Anal. Chem.* 59 (1987) 1984.
- [6] J. Li, *Anal. Chem.* 69 (1997) 4452.
- [7] J. Li, *J. Chromatogr. A* 952 (2002) 63.
- [8] A.B. Littlewood, in: 2nd ed, Gas Chromatography, Principles, Techniques and Applications, Academic Press, New York, 1970.
- [9] J.R. Conder, *J. High. Resolut. Chromatogr. Chromatogr. Commun.* 5 (1982) 341.
- [10] S.C. Pai, *J. Chromatogr. A* 950 (2002) 271.
- [11] G. Taylor, *Proc. R. Soc. Lond. Ser. A* 219 (1953) 186.
- [12] L. Lapidus, N.L. Amundson, *J. Phys. Chem.* 56 (1952) 984.
- [13] S. Golshan-Shirazi, G. Guiochon, in: F. Dondi, G. Guiochon (Eds.), Theoretical Advancement in Chromatography and Related Separation Techniques, Kluwer Academic, Dordrecht, 1991.
- [14] A.J.P. Martin, R.L.M. Synge, *Biochem. J.* 35 (1941) 1358.
- [15] L.C. Craig, *Anal. Chem.* 22 (1950) 1346.
- [16] E. Glueckauf, *Trans. Faraday Soc.* 51 (1955) 34.

- [17] J.S. Fritz, D.M. Scott, *J. Chromatogr.* 271 (1983) 193.
- [18] R. de Levie, *Principles of Quantitative Chemical Analysis*, McGraw-Hill International Editions, 1997.
- [19] R. de Levie, *How to use Excel in Analytical Chemistry and* in *General Scientific Data Analysis*, Cambridge University Press, 2001.
- [20] B. Lin, G. Guiochon, *Theory and Modeling of Nonlinear Chromatography*, Elsevier, Amsterdam, 2003.